

## **General Disclaimer**

### **One or more of the Following Statements may affect this Document**

- This document has been reproduced from the best copy furnished by the organizational source. It is being released in the interest of making available as much information as possible.
- This document may contain data, which exceeds the sheet parameters. It was furnished in this condition by the organizational source and is the best copy available.
- This document may contain tone-on-tone or color graphs, charts and/or pictures, which have been reproduced in black and white.
- This document is paginated as submitted by the original source.
- Portions of this document are not fully legible due to the historical nature of some of the material. However, it is the best reproduction available from the original submission.



## Technical Memorandum 83910

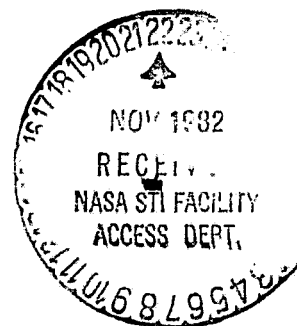
# HIGH FREQUENCY SCATTERING FROM ARBITRARILY ORIENTED DIELECTRIC DISKS

D.M. LeVine, R. Meneghini, R.H. Lang,  
and S.S. Seker

JUNE 1982

National Aeronautics and  
Space Administration

Goddard Space Flight Center  
Greenbelt, Maryland 20771



**HIGH FREQUENCY SCATTERING FROM ARBITRARILY ORIENTED  
DIELECTRIC DISKS**

**D. M. Le Vine and R. Meneghini  
Goddard Space Flight Center  
Greenbelt, Maryland**

**R. H. Lang and S. S. Seker  
Department of Electrical Engineering  
George Washington University  
Washington, DC**

**ABSTRACT**

Calculations have been made of electromagnetic wave scattering from dielectric disks of arbitrary shape and orientation in the high frequency (physical optics) regime. The solution is obtained by approximating the fields inside the disk with the fields induced inside an identically oriented slab (i.e. infinite parallel planes) with the same thickness and dielectric properties. The fields inside the disk excite conduction and polarization currents which are used to calculate the scattered fields by integrating the radiation from these sources over the volume of the disk. This computation has been executed for observers in the far field of the disk in the case of disks with arbitrary orientation and for arbitrary polarization of the incident radiation. The results have been expressed in the form of a dyadic scattering amplitude for the disk. The results apply to disks whose diameter is large compared to wavelength and whose thickness is small compared to diameter, but the thickness need not be small compared to wavelength. Examples of the dependence of the scattering amplitude on frequency, dielectric properties of the disk and disk orientation are presented for disks of circular cross section.

**PRECEDING PAGE BLANK NOT FILMED**

# HIGH FREQUENCY SCATTERING FROM ARBITRARILY ORIENTED DIELECTRIC DISKS

## I. INTRODUCTION

A solution is presented for the scattering from dielectric disks of arbitrary shape and orientation. This work was motivated by an investigation of the effects of leaves on microwave remote sensing of vegetation (Lang, 1981). Determining the scattering and absorption properties of a collection of objects such as leaves requires knowledge of the scattering and absorption properties of the individual objects, and in this work the dielectric disk was adopted as a first order model for leaves. The disk is also of interest as a model to study the scattering and absorption from other particles such as ice crystals in clouds.

Although much work has been done on scattering from perfectly conducting disks (Meixner and Andrejewski, 1950; Andrejewski, 1952; Hodge, 1980; Ruck et. al., 1970), very little has been done on scattering from dielectric disks and disks with non-circular cross section (Ruck, et. al., 1970; Bowman et. al., 1969). However, there has been recent work applicable to thin dielectric disks. Weil and Chu (1976a-b) developed a numerical approximation for the resonant region valid for thin circular disks. This was done by choosing a set of basisfunctions apropos of a thin circular disk and then using a method similar to the moment method to express the induced currents in terms of these basisfunctions. Schiffer and Thielheim (1979) developed a low frequency approximation for the thin dielectric disk by using a Rayleigh type approximation. In this solution the induced currents are found by assuming that the internal fields have the same form as would be obtained in statics. The approximation is valid for disks whose physical cross section is much larger than the thickness and whose thickness is much less than a wavelength. The solution applies at high frequencies (i.e. to disks whose cross section is large compared to wavelength) only if the disk is sufficiently thin.

The work to be described here applies specifically to disks whose cross section is large compared to wavelength but is not restricted to disks which are thin compared to wavelength nor to

disks of circular cross section. The solution is obtained by using a variation of the Kirchoff approximation employed in physical optics scattering from rough surfaces. In this approximation the fields on the surface are approximated by the fields on a plane tangent to the surface. In the application to the disk, the fields inside the disk have been approximated by the fields inside a slab of the same orientation and thickness. Given the fields inside the disk the scattered fields can be obtained from currents induced by these internal fields. In the required integration the cross section of the disk need not be circular nor must the disk be thin compared to wavelength.

In the sections to follow a formal solution for the scattered electric fields is developed in terms of the unknown fields inside the disk. Then the Kirchoff-style approximation for the internal fields is derived for an arbitrarily oriented disk. Using this approximation the volume integration is carried out to obtain explicit forms for the scattered fields for observers in the far field of the disk. Finally, this solution is expressed in the form of a dyadic scattering amplitude for the disk. Examples of the scattering amplitude are presented to illustrate the effects of frequency, dielectric properties and orientation of the disk. Several checks have been made on the solution and are also described. It can be shown that the solution satisfies conservation of energy at high frequencies and that the solution predicts the accepted result for radar cross sections in the special case of normally incident plane waves.

## II. GEOMETRY

The problem to be addressed here is to calculate the fields scattered by a plane wave of arbitrary polarization incident on an arbitrarily oriented disk. The problem is illustrated in Figure 1. The plane wave is assumed to have polarization (direction of the electric field)  $\hat{q}$  and to be propagating in the  $\hat{i}$  direction. Specifying  $\hat{i}$  in terms of the spherical coordinates  $(\theta_i, \phi_i)$  and for convenience letting the incident wave have unit amplitude, one can write:

$$\vec{E}_{inc} = \hat{q} \exp(j k_0 \hat{i} \cdot \vec{r}) \quad (1)$$

where

$$\hat{i} = -\sin(\theta_i) [\cos(\phi_i) \hat{x} + \sin(\phi_i) \hat{y}] - \cos(\theta_i) \hat{z} \quad (2a)$$

and  $k_0 = \omega \sqrt{\epsilon_0 \mu_0}$ . Aside from the requirement  $\hat{q} \cdot \hat{i} = 0$  the unit vector  $\hat{q}$  is arbitrary. The orientation of the disk is described by the Eulerian angles  $(\theta, \phi, \gamma)$  as indicated in Figure 2. (See Goldstein, 1966 and also Appendix B). Starting with the axes of the disk  $(x', y', z')$  aligned with the reference system  $(x, y, z)$  the disk is rotated to its arbitrary position by: 1) rotating  $\phi$  degrees about the  $z' = z$  axis; 2) rotating about the new  $x'$ -axis  $\theta$  degrees; and 3) rotating about the new  $z'$  axis  $\gamma$  degrees. All rotations are counter clockwise. In terms of these angles the normal to the disk,  $\hat{n}$ , is:

$$\hat{n} = \sin \theta [\sin \phi \hat{x} - \cos \phi \hat{y}] + \cos \theta \hat{z} \quad (2b)$$

The shape of the disk is described by the function  $S(\vec{r}')$ , defined in the coordinate system  $(x', y', z')$  fixed on the disk. It is the cross sectional shape looking along the local normal to the disk (i.e.  $z'$  axis). The disk is imagined to be cut from two parallel planes  $T$  meters apart by a cookie cutter with shape  $S(x', y')$ .  $S(x', y') = 1$  on the disk and zero otherwise.

The problem as stated above is sufficiently general to describe scattering from a plane wave of arbitrary polarization and direction of propagation incident on an arbitrarily oriented disk. The orientation of the disk, the shape of the disk,  $S(x', y')$ , its thickness,  $T$ , and its dielectric properties are all arbitrary in the analysis to follow.

### III. THE FORMAL SOLUTION

To obtain a solution for the scattered fields in terms of the fields inside the disk the constitutive relations  $\bar{\mathbf{D}} = \epsilon_0 \bar{\mathbf{E}} + \bar{\mathbf{P}}$  and  $\bar{\mathbf{B}} = \mu_0 (\bar{\mathbf{H}} + \bar{\mathbf{M}})$  are first used to obtain a form of Maxwell's equations with  $\bar{\mathbf{P}}$ ,  $\bar{\mathbf{M}}$  and conduction current,  $\bar{\mathbf{J}}_c$ , as sources. Then, Fourier transforming and introducing the magnetic vector potential,  $\bar{\mathbf{A}}$ , one obtains the wave equation:

$$\nabla^2 \bar{\mathbf{A}} + k_0^2 \bar{\mathbf{A}} = -\mu_0 (\bar{\mathbf{J}}_c - j\omega \bar{\mathbf{P}} + \bar{\nabla} \times \bar{\mathbf{M}}) \quad (3)$$

which has the particular solution

$$\bar{\mathbf{A}}(\mathbf{r}) = \frac{\mu_0}{4\pi} \int [\bar{\mathbf{J}}_c - j\omega \bar{\mathbf{P}} + \bar{\nabla} \times \bar{\mathbf{M}}] \frac{e^{jk_0 R}}{R} d\mathbf{r}' \quad (4)$$

where  $R = |\mathbf{r} - \mathbf{r}'|$  and  $d\mathbf{r}' = dx'dy'dz'$  and the integration is over the volume of the disk. The scattered electric field can be obtained from the vector potential in the form:

$$\bar{\mathbf{E}}(\mathbf{r}') = j\omega [\bar{\mathbf{A}} + \frac{1}{k_0^2} \bar{\nabla} (\bar{\nabla} \cdot \bar{\mathbf{A}})] \quad (5)$$

which yields (Substituting Equation 4 into Equation 5):

$$\mathbf{E}(\mathbf{r}') = j\omega \mu_0 \int_V \bar{\mathbf{J}}_T(\mathbf{r}') \cdot \bar{\mathbf{G}}(\mathbf{r}/\mathbf{r}') d\mathbf{r}' \quad (6)$$

In Equation 6,  $\bar{\mathbf{J}}_T(\mathbf{r}') = \bar{\mathbf{J}}_c - j\omega \bar{\mathbf{P}} + \bar{\nabla} \times \bar{\mathbf{M}}$  and  $\bar{\mathbf{G}}(\mathbf{r}/\mathbf{r}')$  is the dyadic Green's function for free space:

$$\begin{aligned} \bar{\mathbf{G}}(\mathbf{r}/\mathbf{r}') = & \left[ \bar{\mathbf{I}} + \frac{1}{k_0^2} \bar{\nabla} \bar{\nabla} \right] \frac{e^{jk_0 R}}{4\pi R} = \left\{ \left[ 1 + j \frac{1}{k_0 R} - \frac{1}{(k_0 R)^2} \right] \bar{\mathbf{I}} - \right. \\ & \left. - \left[ 1 + j \frac{3}{k_0 R} - \frac{3}{(k_0 R)^2} \right] \bar{\nabla} R \bar{\nabla} R \right\} \frac{e^{jk_0 R}}{4\pi R} \end{aligned} \quad (7)$$

To complete the solution the sources  $\bar{\mathbf{J}}_c$ ,  $j\omega \bar{\mathbf{P}}$  and  $\bar{\nabla} \times \bar{\mathbf{M}}$  are required. In principle, arbitrary relationships between  $\bar{\mathbf{J}}_c$ ,  $\bar{\mathbf{P}}$  and  $\bar{\mathbf{M}}$  and the fields  $\bar{\mathbf{E}}$  and  $\bar{\mathbf{B}}$  can be used; However, for most media important in remote sensing of the earth (e.g. ice, snow, water, vegetation, soil, etc.) it is appropriate to assume a simple linear relationship:

$$\begin{aligned}
\mathbf{J}_c &= \sigma \mathbf{E} \\
\bar{\mathbf{P}} &= \epsilon_0 \chi_e \mathbf{E} \\
\bar{\mathbf{M}} &= \chi_M \mathbf{H}
\end{aligned}
\tag{8}$$

where  $\chi_e$  is the electric susceptibility and  $\chi_M$  the magnetic susceptibility. In most cases  $\chi_M \cong 0$ .

Assuming this to be the case the total current  $\bar{\mathbf{J}}_T$  becomes

$$\bar{\mathbf{J}}_T = -j\omega\epsilon_0 \tilde{\chi}_e \bar{\mathbf{E}} \tag{9}$$

where  $\tilde{\chi}_e$  is an equivalent, complex, electric susceptibility:

$$\tilde{\chi}_e = \chi_e + j\sigma/\omega\epsilon_0 \tag{10}$$

The complex relative permittivity of the medium,  $\tilde{\epsilon}_r$  is:

$$\tilde{\epsilon}_r = \tilde{\chi}_e + 1 \tag{11}$$

$$= \epsilon_r + j\sigma/\omega\epsilon_0 \tag{12}$$

where  $\epsilon_r$  is the relative permittivity of the disk when  $\sigma = 0$ . Substituting Equation 9 into Equation 6, one obtains an expression for the scattered electric field in terms of the electric field  $\bar{\mathbf{E}}(\bar{\mathbf{r}}')$  inside the slab:

$$\mathbf{E}_{\text{scat}}(\bar{\mathbf{r}}) = k_0^2 \int_V \tilde{\chi}_e(\bar{\mathbf{r}}') \bar{\mathbf{E}}(\bar{\mathbf{r}}') \cdot \bar{\mathbf{G}}(\bar{\mathbf{r}}/\bar{\mathbf{r}}') d\bar{\mathbf{r}}' \tag{13}$$



#### IV. THE FIELD INSIDE THE DISK

Equation 13 applies for observation points both inside and outside of the object. If the observer is inside the object, then Equation 13 is an integral equation for  $\bar{E}(\bar{r})$ . When the observer is outside, then Equation 13 is a solution for the fields scattered by the object in terms of the fields inside the object. The problem, of course, is that the fields inside the object are not known in either case, and approximations are necessary. The approximation to be used here will be to assume that the fields inside the disk are the same as would exist in a slab of infinite parallel faces of the same thickness and orientation. This is an approximation which ought to be reasonable for disks whose cross section is large compared to wavelength and thickness and is independent of the dielectric constant of the medium. It is the analogue of the tangent plane (Kirchhoff) approximation employed in the physical optics approach to scattering from surfaces.

The fields inside the equivalent slab are most easily obtained in the coordinate system  $(x'y'z')$  fixed on the disk. Once obtained they can then be expressed in terms of the reference coordinates  $(x,y,z)$  by a suitable transformation of coordinates. The problem as seen in the coordinate system fixed on the disk is shown in Figure 3. Notice that the origin of the primed coordinate system is at the center of the slab and that the plane wave is incident from the arbitrary direction,  $\hat{i}$ . As seen by an observer on the slab the incident plane wave has the form:

$$\bar{E}_{inc}(\bar{r}') = \hat{q} e^{jk_o \hat{i} \cdot \bar{r}'} \quad (14)$$

where primes (') are being used to remind the reader that these are coordinates in the reference frame of the disk. To find the fields inside the slab, it is convenient to resolve the incident wave into its horizontally and vertically polarized components as seen by an observer on the slab. Letting  $\hat{h}$  and  $\hat{v}$  be the appropriate unit vectors in the slab's reference system, one can write  $\hat{q}$  in terms of its projections on these polarization vectors:  $\hat{q} = (\hat{q} \cdot \hat{h})\hat{h} + (\hat{q} \cdot \hat{v})\hat{v}$ . With this notation a unit amplitude incident wave, as seen by the observer on the slab, can be written:

$$\bar{E}_{inc}(\bar{r}') = [(\hat{q} \cdot \hat{h})\hat{h} + (\hat{q} \cdot \hat{v})\hat{v}] e^{jk_o \hat{i} \cdot \bar{r}'} \quad (15)$$

The fields inside the slab are also plane waves. Explicitly separating their dependence on the coordinate perpendicular to the slab ( $z'$ ) and coordinate parallel to the slab boundaries ( $x', y'$ ), they can be written in the form:

$$\bar{E}_{\text{slab}}(\mathbf{r}') = \bar{E}_+(x', y') e^{j(nk_0 K'_z)z'} + \bar{E}_-(x', y') e^{-j(nk_0 K'_z)z'} \quad (16a)$$

where

$$\bar{E}_{\pm}(x', y') = \bar{e}_{\pm} e^{jn k_0 [K'_x x' + K'_y y']} \quad (16b)$$

$n$  is the index of refraction of the medium in the slab ( $n = \sqrt{\epsilon_r}$ ) and  $\mathbf{K} = K'_x \hat{x}' + K'_y \hat{y}' + K'_z \hat{z}'$  is a unit vector in the direction of propagation of the wave inside the slab which propagates in the  $+z$ -direction (i.e.  $K'_z > 0$ ). The vector amplitudes  $\bar{e}_{\pm}$  of the waves inside the slab can also be resolved into horizontally and vertically polarized components. Thus, let  $\hat{h}_{\epsilon}^{\pm}$ ,  $\hat{v}_{\epsilon}^{\pm}$  be unit vectors in the direction of the electric field inside the slab when the slab is excited by an incident horizontally or vertically polarized wave, respectively. (For example, if  $\hat{q} = \hat{h}$  then the waves inside the slab will have polarization  $\hat{h}_{\epsilon}^{\pm}$ .) Also let the (scalar) amplitude of the waves inside the slab due to an incident horizontally or vertically polarized wave of unit amplitude be  $e_{\text{h}}^{\pm}$ ,  $e_{\text{v}}^{\pm}$  respectively. Then, in the case of an incident wave of arbitrary polarization  $\hat{q}$  one can write the amplitude of the waves inside the slab as

$$\bar{e}_{\pm} = (\hat{q} \cdot \hat{h}) e_{\text{h}}^{\pm} \hat{h}_{\epsilon}^{\pm} + (\hat{q} \cdot \hat{v}) e_{\text{v}}^{\pm} \hat{v}_{\epsilon}^{\pm} \quad (17)$$

The scalars  $e_{\text{h},\text{v}}^{\pm}$  are characteristics of the slab, independent of its orientation. They are obtained from the boundary conditions at the slab interfaces in the same manner as is conventional in finding the reflection or transmission coefficients (e.g. Born and Wolf, 1959). One obtains:

$$e_{\text{h},\text{v}}^+ = \frac{t_{\text{h},\text{v}} r_{\text{h},\text{v}} e^{j\psi}}{1 - r_{\text{h},\text{v}}^2 e^{j\psi}} e^{-j\Delta^+} \quad (18a)$$

$$e_{\text{h},\text{v}}^- = \frac{t_{\text{h},\text{v}}}{1 - r_{\text{h},\text{v}}^2 e^{j\psi}} e^{-j\Delta^-} \quad (18b)$$

where

$$\psi = 2k_0 T n K'_z \quad (19a)$$

$$\Delta^\pm = \frac{1}{2}k_0 T [-i'_z \pm nK'_z] \quad (19b)$$

$$r_{h,v} = \frac{1 - \lambda_{h,v}}{1 + \lambda_{h,v}} \quad (19c)$$

$$t_{h,v} = \frac{2}{1 + \lambda_{h,v}} \sqrt{\frac{\lambda_{h,v}}{\lambda_h}} \quad (19d)$$

$$\lambda_h = -n \frac{K'_z}{i'_z} \quad (19e)$$

$$\lambda_v = -\frac{1}{n} \frac{K'_z}{i'_z} \quad (19f)$$

where  $K'_z = \hat{K} \cdot \hat{n} > 0$  and  $i'_z = \hat{i} \cdot \hat{n} < 0$ ; and the  $r_{h,v}$  and  $t_{h,v}$  are the reflection and transmission coefficients, respectively, of a half-space with the same dielectric properties as the disk. The minus sign (-) in Equations 19e, f are the result of the convention adopted here for  $\hat{i}$  and  $\hat{n}$  (i.e. the wave is incident on the slab from the  $\hat{n}$  side).

## V. THE SCATTERED FIELD

The fields scattered from the disk can now be obtained by substituting the fields inside the disk (Equations 16) into Equation 13. To do the integration in Equation 13 over the volume of the disk it will be assumed that the observer is many wavelengths from the disk ( $k_0 R \gg 1$ ) and that the disk is small compared to the distance between the disk and the observer (e.g.  $L/R \ll 1$  and  $kL^2/R \ll 2\pi$  where  $L$  is a dimension characteristic of the size of the disk). In this case one can approximate the Green's function by:

$$\bar{G}(\bar{r}/\bar{r}') \approx (\bar{I} - \hat{o} \hat{o}) \frac{e^{ik_0(R_0 - \hat{o} \cdot \bar{r}')}}{4\pi R_0} \quad (20)$$

where  $R_0$  is the distance from the center of the disk to the observer and  $\hat{o}$  is a unit vector from the origin to the observer (i.e. in the direction of propagation of the wave scattered to the observer). Substituting Equation 16 into Equation 13, using Equation 20, and separately doing the integration over the  $(x', y')$  and  $z'$  coordinates one obtains the following expression for the fields scattered from homogeneous disks ( $\chi_e$  and  $\sigma$  constant):

$$\bar{E}_{\text{scat}}(\hat{q}) = k_0^2 \tilde{\chi}_e \frac{e^{ik_0 R_0}}{4\pi R_0} \bar{R}(T) \tilde{S}(\bar{\nu}'_t) \quad (21)$$

where

$$\bar{R}(T) = \int_{-T/2}^{T/2} \hat{o} \times \left\{ \left[ \bar{e}_+ e^{jk_0 [nK'_z - o'_z] z'} + \bar{e}_- e^{-jk_0 [nK'_z + o'_z] z'} \right] \times \hat{o} \right\} dz' \quad (22a)$$

$$= T \left\{ \hat{o} \times [\bar{e}_+ \times \hat{o}] \text{sinc} \left[ \frac{1}{2} k_0 T (nK'_z - o'_z) \right] + \hat{o} \times [\bar{e}_- \times \hat{o}] \text{sinc} \left[ \frac{1}{2} k_0 T (nK'_z + o'_z) \right] \right\} \quad (22b)$$

$$\tilde{S}(\bar{\nu}'_t) = \int_{-\infty}^{\infty} \int_{-\infty}^{\infty} S(\bar{r}'_t) e^{j2\pi \bar{\nu}'_t \cdot \bar{r}'_t} d\bar{r}'_t \quad (22c)$$

The subscript "t" in Equation 22c denotes transverse components:  $\bar{r}'_t = x' \hat{x}' + y' \hat{y}'$

and  $\bar{\nu}'_t = \frac{k_0}{2\pi} [n\bar{K}'_t - \bar{o}'_t] = \frac{k_0}{2\pi} \hat{n} \times [n\bar{K} - \hat{o}] \times \hat{n}$ . Notice that using Snell's law at the slab

boundaries,  $n \bar{K}'_t = \hat{i}'_t$ , so that one can write  $\bar{\nu}'_t$  in terms of  $\hat{i}$  and  $\hat{o}$  :

$$\bar{\nu}'_t = \frac{k_o}{2\pi} \hat{n} \times [(\hat{i} - \hat{o}) \times \hat{n}] \quad (22d)$$

The vector direction of the scattered field,  $\bar{E}_{scat}$ , is determined by the vectors  $\hat{o} \times (\bar{e}_{\pm} \times \hat{o})$  associated with  $\bar{R}(T)$ . Since  $\hat{o}$  is a unit vector in the direction of propagation of the scattered field (i.e. pointing from the disk to the observer), the scattered fields are clearly transverse as seen by the observer. This is as expected since a far field limit has been taken to obtain the solution.

It is conventional to express the scattered fields in terms of their vertically and horizontally polarized components. To do so, let  $\hat{p}$  be a unit vector in the direction of vertical or horizontal polarization (defined by the observer). Then  $\hat{p} \cdot \bar{E}_{scat}(\hat{q})$  is the scattered electric field of polarization  $\hat{p}$  due to an incident wave of polarization  $\hat{q}$  (as defined at the transmitting antenna). Noting that  $\hat{p} \cdot [\hat{o} \times (\bar{e}_{\pm} \times \hat{o})] = \hat{p} \cdot \bar{e}_{\pm}$  and using Equation 17 for  $\bar{e}_{\pm}$  one can write:

$$\hat{p} \cdot \bar{E}_{scat}(\hat{q}) = [\hat{p} \cdot \bar{F}(\hat{i}, \hat{o}) \cdot \hat{q}] T k_o^2 \tilde{\chi}_e \tilde{S}(\nu'_t) \frac{e^{jk_o R_o}}{4\pi R_o} \quad (23)$$

where the dyadic  $\bar{F}(\hat{i}, \hat{o})$  has the form:

$$\begin{aligned} \bar{F}(\hat{i}, \hat{o}) = & [\hat{h}_e \hat{h} e_h^- + \hat{v}_e^- \hat{v} e_v^-] \text{sinc} [1/2 k_o T (nK'_z - o'_z)] + \\ & + [\hat{h}_e^+ \hat{h} e_h^+ + \hat{v}_e^+ \hat{v} e_v^+] \text{sinc} [1/2 k_o T (nK'_z - o'_z)] \end{aligned} \quad (24)$$

Equation 23 suggests the definition of a dyadic scattering amplitude  $\bar{f}(\hat{i}, \hat{o})$ :

$$\bar{f}(\hat{i}, \hat{o}) = \frac{T k_o^2 \tilde{\chi}_e}{4\pi} \tilde{S}(\nu'_t) \bar{F}(\hat{i}, \hat{o}) \quad (25)$$

To complete the solution it is necessary to find explicit expressions for the polarization vectors  $\hat{v}_e^{\pm}$ ,  $\hat{h}_e^{\pm}$  and  $\hat{v}$ ,  $\hat{h}$  associated with the slab and with  $\hat{q}$ ,  $\hat{p}$  associated with the incident and scattered waves. To do so the following definitions will be adopted: A horizontally polarized wave (h) is one whose electric field is perpendicular to the plane of incidence (plane defined by the

z-axis and the direction of propagation) and a vertically polarized wave (v) is one whose electric field is parallel to the plane of incidence. In addition,  $\hat{v}$ ,  $\hat{h}$ ,  $\hat{k}$  form a right hand orthogonal set where  $\hat{k}$  is a unit vector in the direction of propagation of the waves:  $\hat{v} \times \hat{h} = \hat{k}$ . With these definitions, one may write explicit forms for the polarization vectors in the reference coordinate system. Thus, for the incident wave (i.e.  $\hat{q} = \hat{h}_i$  or  $\hat{v}_i$ ) one has:

$$\hat{h}_i = \frac{\hat{i} \times \hat{z}}{|\hat{i} \times \hat{z}|} \quad (26a)$$

$$\hat{v}_i = \hat{h}_i \times \hat{i} \quad (26b)$$

where  $\hat{i}$  is defined in terms of the spherical coordinates  $(\theta_i, \phi_i)$ :

$$\hat{i} = -\sin \theta_i [\cos \phi_i \hat{x} + \sin \phi_i \hat{y}] - \cos \theta_i \hat{z} \quad (26c)$$

and in the case of the scattered fields the unit vectors  $\hat{h}_s$ ,  $\hat{v}_s$  in the direction of horizontal and vertical polarization ( $\hat{q} = \hat{h}_s$  or  $\hat{v}_s$ ) are:

$$\hat{h}_s = \frac{\hat{o} \times \hat{z}}{|\hat{o} \times \hat{z}|} \quad (27a)$$

$$\hat{v}_s = \hat{h}_s \times \hat{o} \quad (27b)$$

where the spherical coordinates  $(\theta_s, \phi_s)$  have been adopted to define  $\hat{o}$ :

$$\hat{o} = \sin \theta_s [\cos \phi_s \hat{x} + \sin \phi_s \hat{y}] + \cos \theta_s \hat{z} \quad (27c)$$

The unit vectors  $\hat{h}$ ,  $\hat{v}$  are the direction of horizontal and vertical polarization as defined by an observer on the slab but expressed in terms of the reference coordinate system (unprimed). Since  $\hat{n} = \hat{z}'$  as seen in the reference system and since the direction of propagation of the incident wave as seen in the reference frame is  $\hat{i}$ , one obtains:

$$\hat{h} = \frac{\hat{i} \times \hat{n}}{|\hat{i} \times \hat{n}|} \quad (28a)$$

$$\hat{v} = \hat{h} \times \hat{i} \quad (28b)$$

where the normal to the slab  $\hat{n}$  is defined by the Eulerian angles  $(\theta, \phi, \gamma)$ :

$$\hat{n} = \sin \theta [\sin \phi \hat{x} - \cos \phi \hat{y}] + \cos \theta \hat{z} \quad (28c)$$

The unit vectors  $\hat{h}_e^\pm \hat{v}_e^\pm$  for the direction of electric field inside the slab are also required. Letting  $\hat{K}_\pm$  be a unit vector in the direction of propagation of the two waves inside the slab one has:

$$\hat{h}_e^\pm = \frac{\hat{K}_\pm \times \hat{n}}{|\hat{K}_\pm \times \hat{n}|} \quad (29a)$$

$$\hat{v}_e^\pm = \hat{h}_e^\pm \times \hat{K}_\pm \quad (29b)$$

It is shown in Appendix A that

$$\hat{K}_\pm = \frac{1}{n} [\hat{i} + \Omega_\pm \hat{n}] \quad (30a)$$

where

$$\Omega_\pm = -(\hat{i} \cdot \hat{n}) \pm \sqrt{(n^2 - 1) + (\hat{i} \cdot \hat{n})^2} \quad (30b)$$

Thus one obtains:

$$\hat{h}_e^\pm = \hat{h} \quad (31a)$$

$$\hat{v}_e^\pm = \frac{1}{n} [\hat{v} + \Omega_\pm \hat{h} \times \hat{n}] = \frac{1}{n} [\hat{v} + \bar{\Omega}_\pm] \quad (31b)$$

With the polarization unit vectors given above one can write the solution for the scattered field in the final form:

$$\hat{p} \cdot \vec{E}_{\text{scat}}(\hat{q}) = [\hat{p} \cdot \vec{f}(\hat{i}, \hat{o}) \cdot \hat{q}] \frac{e^{jk_0 R_0}}{R_0} \quad (32a)$$

$$\vec{f}(\hat{i}, \hat{o}) = \frac{1}{4\pi} T k_0^2 \tilde{\chi}_e \tilde{S}(\mathcal{P}') \vec{F}(\hat{i}, \hat{o}) \quad (32b)$$

$$\begin{aligned} \vec{F}(\hat{i}, \hat{o}) = & [\hat{h} \hat{h} e_{\hat{n}}^- + \frac{1}{n} (\hat{v} + \bar{\Omega}_-) \hat{v} e_{\hat{v}}^-] \text{sinc} [\frac{1}{2} k_0 T(nK'_2 + o'_2)] \\ & + [\hat{h} \hat{h} e_{\hat{n}}^+ + \frac{1}{n} (\hat{v} + \bar{\Omega}_+) \hat{v} e_{\hat{v}}^+] \text{sinc} [\frac{1}{2} k_0 T(nK'_2 - o'_2)] \end{aligned} \quad (32c)$$

where the  $e_{\hat{h},v}^{\pm}$  are given by Equations 18 and 19 and

$$i'_z = \hat{i} \cdot \hat{n} = -\sin \theta_i \sin \theta \sin (\phi - \phi_i) - \cos \theta_i \cos \theta \quad (33a)$$

$$o'_z = \hat{o} \cdot \hat{n} = \sin \theta_s \sin \theta \sin (\phi - \phi_s) + \cos \theta_s \cos \theta \quad (33b)$$

$$nK'_z = n\hat{K} \cdot \hat{n} = \sqrt{(n^2 - 1) + (\hat{i} \cdot \hat{n})^2} \quad (33c)$$

$$\bar{\Omega}_{\pm} = (-i'_z \pm nK'_z) \hat{n} \times \hat{n} \quad (33d)$$

Explicit forms for the shape function  $\tilde{S}(v'_i)$  are given in Appendix C.



## VI. EXAMPLES

Examples of the scattering amplitude will be presented in this section for a sample disk to illustrate some of the characteristics of Equations 32. Calculations have been made to illustrate effects of frequency, disk orientation and dielectric constant on the scattered fields. The calculations are for a nominal disk of radius 10 cm and thickness 0.5 cm, and except where indicated the frequency of the incident radiation is 9 GHz and the dielectric constant of the disk is  $\epsilon_r = 25 + j11$  which is representative of leaves in the microwave region. In these examples the incident radiation has been chosen so that the direction of incidence is in the y-z plane  $30^\circ$  from the z-axis ( $\hat{i} = -\cos(30^\circ)\hat{z} - \sin(30^\circ)\hat{y}$ ) and the normal to the disk,  $\hat{n}$ , is in the plane of incidence ( $\hat{n} = -\sin\theta \hat{y} + \cos\phi \hat{z}$ ). The geometry is shown in Figure 4. To do the calculations the observer is imagined to be on the surface of a large sphere centered on the origin and the scattering amplitude  $\hat{p} \cdot \bar{f}(\hat{i}, \hat{o}) \cdot \hat{q}$  is computed as the observer is moved around one of the great circles formed by passing a plane through the z-axis. The magnitude of the scattering amplitude,  $|\hat{p} \cdot \bar{f}(\hat{i}, \hat{o}) \cdot \hat{q}|$ , has been displayed as a polar plot of amplitude versus angle on the great circle (Figures 4-15). In each case the top of the figure corresponds to the point when the observer is on the z-axis. When the observer is in the plane of incidence, (e.g. Figures 6 - 15) backscatter occurs at  $30^\circ$  to the right of the top and forward scatter at  $150^\circ$  to the left. The polar plots are all linear in amplitude. The outer circle represents  $|\hat{p} \cdot \bar{f}(\hat{i}, \hat{o}) \cdot \hat{q}| = 1.0$  and the inner circle is  $|\hat{p} \cdot \bar{f}(\hat{i}, \hat{o}) \cdot \hat{q}| = 0.2$ . This scale is the same in all the examples to be presented here (Figures 5-15) except for the  $45^\circ$  and  $90^\circ$  cuts in Figure 5 where the outer circle was chosen to be  $|\hat{p} \cdot \bar{f}(\hat{i}, \hat{o}) \cdot \hat{q}| = .05$  to better show the detail of these small scattered fields.

The elements of the scattering amplitude most commonly of interest are:

$$\hat{h}_s \cdot \bar{f}(\hat{i}, \hat{o}) \cdot \hat{h}_i = f_{hh}$$

$$\hat{v}_s \cdot \bar{f}(\hat{i}, \hat{o}) \cdot \hat{h}_i = f_{vh}$$

$$\hat{h}_s \cdot \bar{f}(\hat{i}, \hat{o}) \cdot \hat{v}_i = f_{hv}$$

$$\hat{v}_s \cdot \bar{f}(\hat{i}, \hat{o}) \cdot \hat{v}_i = f_{vv}$$

The elements  $f_{hh}$  and  $f_{vh}$  are proportional to the horizontal and vertical polarized scattered field, respectively (as seen by the observer), due to an incident wave of horizontal polarization. The elements,  $f_{hv}$  and  $f_{vv}$  are proportional to the scattered field of horizontal and vertical polarization, respectively, due to a vertically polarized incident wave. The unit vectors,  $\hat{h}_i, \hat{v}_i$  and  $\hat{h}_s, \hat{v}_s$  are indicated in Figure 4 for reference. The magnitude of these four components of the scattering amplitude have been calculated.

Figure 5 shows the four components of the scattering amplitude  $f_{hh}, f_{vh}, f_{hv}$  and  $f_{vv}$  for an observer in the plane of incidence ( $0^\circ$ ), in a plane perpendicular to the plane of incidence ( $90^\circ$ ) and in a plane half way between these two ( $45^\circ$ ). (See Figure 4.) The calculations are for the case  $\hat{n} = \hat{z}$ . Each plot indicates the magnitude of  $\hat{p} \cdot \vec{f}(\hat{i}, \hat{o}) \cdot \hat{q}$  in polar form with the z-axis at the top of the polar plot. Notice that  $f_{vh} = f_{hv} = 0$  when the observer and  $\hat{n}$  are in the plane of incidence ( $0^\circ$ ). That is, there is no depolarization in this case. This is true whenever  $\hat{o}, \hat{n}$  and  $\hat{i}$  are coplanar. Also notice that  $f_{hh} = 0$  when the observer is in a plane perpendicular to the plane of incidence. This is a coincidence dependent on the definitions chosen for the polarization unit vectors. In the plane of incidence ( $0^\circ$ ), the scattering amplitude has two major peaks, one in the direction of incidence,  $\hat{i}$ , (the downward pointing peaks in Figure 5) and one in the specular direction (the upward pointing peaks). The specular peak is in the direction of radiation reflected from an identically oriented infinite slab and the downward or "forward scattered" peak is in the direction of radiation transmitted through such a slab. For a highly conducting disk, the forward scattered radiation combines with the incident field to produce a "shadow" behind the disk.

In the physical optics regime the shape and amplitude of the forward scatter and specular peaks depend on the product,  $ka = 2\pi a/\lambda$  where  $a$  is the radius of the disk and  $\lambda$  is the wavelength of the incident radiation in the ambient medium (Appendix C). This is illustrated in Figures 6-7 which show  $f_{hh}$  and  $f_{vv}$  (respectively) for several values of  $ka$ . The geometry is as illustrated in Figure 4 with the observer in the plane of incidence ( $0^\circ$  plane). Notice that as  $ka$  increase the peaks become larger and narrower in the directions of the reflected and transmitted waves. For a circular

disk, the peaks behave like  $J_1(x)/x$  where  $J_1(x)$  is a Bessel function of first kind and  $x$  depends on  $ka$  and disk orientation (Appendix C).

Changing the orientation of the disk affects the direction and shape of the peaks. This is illustrated in Figures 8 ( $f_{hh}$ ) and 9 ( $f_{vv}$ ) for the special case where  $\hat{o}, \hat{n}, \hat{i}, \hat{z}$  are all coplanar. In these examples the observer is in the  $0^\circ$  plane (Figure 4) and  $\hat{n}$  is also in the  $0^\circ$  plane but at several different angles with respect to the incident wave. The four polar plots have been obtained with  $\hat{n}$  parallel to  $\hat{i}$  ( $\theta = 0^\circ$ ) and then moved to the left so that the angle between  $\hat{n}$  and  $\hat{i}$  is  $15^\circ$ ,  $45^\circ$  and finally  $60^\circ$ . Notice that as the direction of  $\hat{n}$  is changed the specular peak changes direction but that a peak always remains in the forward scatter direction. As the disk appears more edge on to the incident radiation ( $\theta > 60^\circ$ ) the specular and forward scatter peaks merge and their amplitude decreases toward zero. (The theory is not applicable near grazing incidence.)

The effect of the dielectric constant of the disk on the scattered fields is illustrated in Figures 10-15. The geometry is as illustrated in Figure 4 with the observer in the  $0^\circ$  plane and  $\hat{n} = \hat{z}$ . The frequency is 9 GHz ( $ka = 2$ ). Figures 10 and 11 are for a lossless dielectric ( $\tilde{\epsilon}_r$  real) and show the effect on  $f_{hh}$  and  $f_{vv}$ , respectively, of increasing the relative dielectric constant of the disk. With the chosen frequency (9 GHz) and thickness (0.5 cm) the disk goes through a quarter wave resonance near  $\tilde{\epsilon}_r = 11$ . These figures show the effects on the scattering amplitude of increasing  $\tilde{\epsilon}_r$  from 1.0 (upper left) through resonance and then to large, non-resonant values. Initially the scattered radiation increases as  $\tilde{\epsilon}_r$  increases; however, near the resonant condition,  $\tilde{\epsilon}_r = 11$ , the reflected radiation decreases markedly. The forward scatter peak, on the other hand, is only slightly affected and appears to increase somewhat near resonance. This pattern of decreasing specular peak occurs at all quarter wave resonances, which for this disk ( $T = 0.5$  cm) and frequency (9 GHz) occur at  $\tilde{\epsilon}_r = 11, 44, 99$ , etc. For large values of  $\tilde{\epsilon}_r$  not near resonance the scattering amplitude approaches a limiting shape as illustrated by the last two examples in Figures 10 and 11 ( $\tilde{\epsilon}_r = 70$  and 1000).

The presence of loss in the dielectric significantly affects the behaviour of the scattered fields near resonance. With even small amounts of loss, the resonance is virtually eliminated. This is illustrated in Figures 12 and 13 which show examples of the scattering amplitude  $f_{hh}$  and  $f_{vv}$ , respectively for the nominal disk with fixed loss ( $\text{Im } \tilde{\epsilon}_r = 2$ ) and with the real part of  $\tilde{\epsilon}_r$  having values near the quarter wave resonance at  $\tilde{\epsilon}_r = 11$ . For values of  $\text{Im } \tilde{\epsilon}_r$  less than 2 a decrease in the specular peak is noticeable and for values of  $\text{Im } \tilde{\epsilon}_r$  greater than 2 the resonance is even less apparent than in Figures 12 and 13.

Figures 14 and 15 present examples of the scattering amplitude for the nominal disk with a purely lossy dielectric:  $\text{Re } \tilde{\epsilon}_r = 0$ . Four examples illustrating the effects of increasing  $\text{Im } \tilde{\epsilon}_r = \epsilon''$  are shown. The behaviour is very much like increasing  $\text{Re } \tilde{\epsilon}_r$  except for the lack of resonances. The scattering amplitude quickly reaches a limiting value and is essentially independent of  $\tilde{\epsilon}_r$  for  $\epsilon'' \gtrsim 10$ .

## VII. NORMAL INCIDENCE

The special case in which the radiation is normally incident on the disk provides a check on the solution. In this case one expects the horizontally polarized radiation scattered from horizontally polarized incident radiation to equal the vertically polarized radiation scattered from vertically polarized incident radiation, and that there will be no cross polarized scattered radiation. That is, one expects:

$$\begin{aligned} f_{hh} &= f_{vv} \\ f_{hv} &= f_{vh} = 0 \end{aligned}$$

Also, at normal incidence one expects the backscatter cross section,  $\sigma_N$  to be

$$\sigma_N = R_n^2 \sigma_\infty$$

where  $\sigma_\infty$  is the backscatter cross section of a perfectly conducting disk and  $R_n$  is the reflection coefficient of a slab of the same thickness as the disk (Ruck et al., 1970). It will be shown that these results are obtained from the solutions developed here.

At normal incidence  $\hat{n} = \hat{z}$  and  $\hat{h} \times \hat{n} = \hat{v}$ , and consequently, the dyadic  $\overline{\overline{F}}(\hat{i}, \hat{o})$  has the simple form:

$$\overline{\overline{F}}(\hat{i}, \hat{o}) = \hat{h}\hat{h} [e_h^- \text{sinc}(\theta^+) + e_h^+ \text{sinc}(\theta^-)] + \hat{v}\hat{v} [e_v^+ \text{sinc}(\theta^-) - e_v^- \text{sinc}(\theta^+)] \quad (34a)$$

where

$$\theta^\pm = \frac{1}{2}k_0 T [nK'_2 \pm o'_2] = \frac{1}{2}k_0 T [n \pm 1] \quad (34b)$$

The polarization vectors at normal incidence are  $\hat{h}_s = \hat{h}_i = \hat{h}$  and  $-\hat{v}_s = +\hat{v}_i = +\hat{v}$  where the minus sign (-) in the vertical polarized scattered radiation  $\hat{v}_s$  is a consequence of the convention chosen for polarization ( $\hat{v}_s = \hat{h}_s \times \hat{o}$ ) and the fact that a normal incidence  $\hat{i} = -\hat{o}$ . With these polarization vectors one has:

$$\begin{aligned} \hat{h}_s \cdot \overline{\overline{F}} \cdot \hat{h}_i &= e_h^- \text{sinc}(\theta^+) + e_h^+ \text{sinc}(\theta^-) \\ \hat{h}_s \cdot \overline{\overline{F}} \cdot \hat{v}_i &= 0 \\ \hat{v}_s \cdot \overline{\overline{F}} \cdot \hat{h}_i &= 0 \\ \hat{v}_s \cdot \overline{\overline{F}} \cdot \hat{v}_i &= e_v^- \text{sinc}(\theta^+) - e_v^+ \text{sinc}(\theta^-) \end{aligned} \quad (35)$$

Clearly  $f_{hv} = f_{vh} = 0$  at normal incidence. To determine the like-polarized components of scattered electric field,  $f_{hh}$  and  $f_{vv}$ , note that at normal incidence

$$e_{h,v}^+ = -r_{h,v} e^{jk_0 T n} e_{h,v}^- \quad (36a)$$

$$r_h = \frac{1-n}{1+n} = -r_v \quad (36b)$$

and also that the reflection coefficients  $R_{h,v}$  of a slab of thickness  $T$  which in the notation adopted here are:

$$R_{h,v} = \frac{1}{2} \left[ (1 + \lambda_{h,v}) e_{h,v}^+ e^{j\Delta^+} + (1 - \lambda_{h,v}) e_{h,v}^- e^{j\Delta^-} \right] \sqrt{\frac{\lambda_h}{\lambda_{h,v}}} e^{-jk_0 T} \quad (37)$$

have the following form at normal incidence

$$R_h = \frac{1}{2} [(1+n) e_h^+ e^{j\alpha n} + (1-n) e_h^- e^{-j\alpha n}] e^{-j\alpha} \quad (38a)$$

$$R_v = \frac{1}{2} [(1+n) e_v^+ e^{j\alpha n} - (1-n) e_v^- e^{-j\alpha n}] e^{-j\alpha} \quad (38b)$$

where  $\alpha = \frac{1}{2} k_0 T$ . Now substituting Equations 36 into Equations 35 and using Equations 38 one obtains:

$$\hat{h}_s \cdot \vec{F} \cdot \hat{h}_i = -j \frac{2}{(k_0 T)(n^2-1)} R_h \quad (39a)$$

$$\hat{v}_s \cdot \vec{F} \cdot \hat{v}_i = -j \frac{2}{(k_0 T)(n^2-1)} R_v \quad (39b)$$

And since  $R_h = -R_v = R_n$  it is clear that  $f_{hh} = -f_{vv}$ . The sign difference between  $f_{hh}$  and  $f_{vv}$  is a consequence of the convention chosen for polarization: vertical polarization for scattered and incident waves along the same line of sight are in opposite directions.

The radar cross section at normal incidence is readily obtained from the preceding results and also provides a check on the solution. Recalling that the definition of radar cross section at normal incidence is

$$\sigma_N = \lim_{R \rightarrow \infty} 4\pi R^2 \frac{[\mathbf{F}_{pp} \cdot \mathbf{E}_{pp}^*]}{[\mathbf{E}_p \cdot \mathbf{E}_p^*]} \quad (40)$$

one obtains

$$\sigma_N = |\hat{\mathbf{p}}_s \cdot \mathbf{F} \cdot \hat{\mathbf{p}}_i|^2 \frac{(Tk_0^2)^2}{4\pi} [\tilde{\chi}_e \tilde{\mathbf{S}}(\hat{\mathbf{v}}_i)]^2 \quad (41)$$

Now using the result that  $n^2 - 1 = \tilde{\chi}_e$  and that at normal incidence  $\tilde{\mathbf{S}}(\hat{\mathbf{v}}_i) = S_0$  where  $S_0$  is the area of the disk (Appendix C) one obtains:

$$\sigma_N = \frac{k_0^2 S_0^2}{\pi} |R_n|^2 \quad (42)$$

The radar cross section of a perfectly conducting disk at normal incidence is  $\sigma_\infty = k_0^2 S_0^2/\pi$  and so the radar cross section of the dielectric disk at normal incidence can be written

$$\sigma_N = |R_n|^2 \sigma_\infty \quad (43)$$

which agrees with the expected result (Ruck, et al., 1971).

This result is especially simple for thin disks. ( $k_0 T n \ll 1$ ). Keeping only lowest terms in  $k_0 T$  in Equation 38 one can show that

$$R_N \cong j \frac{k_0 T}{4} (n^2 - 1) \quad (44)$$

and so at normal incidence

$$\sigma_N \cong \left(\frac{k_0 T}{4}\right)^2 |n^2 - 1|^2 \sigma_\infty = k_0^4 \frac{(TS_0)^2}{16\pi} |n^2 - 1|^2 \quad (45)$$

That is, the thin disk at normal incidence is Rayleigh-like, scattering power proportional to  $1/\lambda^4$  rather than as  $1/\lambda^2$  as the perfectly conducting disk would suggest.

## VIII. ENERGY CHECK

A check has been made to see if the solution for the scattered fields conserves energy. This has been done by showing that the solution satisfies the "optical theorem". The optical theorem relates the total power scattered ( $P_s$ ) and absorbed ( $P_a$ ) to the scattering amplitude in the forward direction (Born and Wolf, 1959). One can state the optical theorem as follows:

$$P_s + P_a = P_i \frac{4\pi}{k_0} \text{Im}[\hat{q} \cdot \bar{\Gamma}(i,i) \cdot \hat{q}] \quad (46)$$

where  $P_i$  is the power density of the incident wave,  $\hat{i}$  is a unit vector in the direction of propagation of the incident wave, and  $\hat{q}$  is a unit vector in the direction of polarization of the electric field of the incident wave. Defining scattering and absorption cross sections by  $\sigma_s = P_s/P_i$  and  $\sigma_a = P_a/P_i$  respectively, the optical theorem becomes:

$$\sigma_s + \sigma_a = \frac{4\pi}{k_0} \text{Im} [\hat{q} \cdot \bar{\Gamma}(i,i) \cdot \hat{q}] \quad (47)$$

where

$$\sigma_s = \frac{P_s}{P_i} = \iint_{\text{Sphere}} [\bar{\Gamma}(i,\theta) \cdot \hat{q}] \cdot [\bar{\Gamma}(i,\theta) \cdot \hat{q}]^* d\Omega \quad (48a)$$

$$\sigma_a = \frac{P_a}{P_i} = \sqrt{\frac{\mu_0}{\epsilon_0}} \iiint_{\text{disk}} \sigma \bar{E} \cdot \bar{E}^* dv \quad (48b)$$

the integration in the expression for  $\sigma_s$  is over solid angle  $d\Omega = \sin\theta d\theta d\phi$  and the fields  $\bar{E}$  in the expression for  $\sigma_a$  are the fields inside the disk produced by a unit amplitude incident plane wave. They are given in the reference frame fixed on the disk by Equations 16 in the text. For purposes of doing the energy check, the orientation of the disk is unimportant and can be chosen for convenience; the choice in which the primed and unprimed systems are identical is most convenient ( $\theta = \phi = \gamma = 0$ ). In this case, using Equations 16 in Equation 48b one obtains:

$$\sigma_a = S_0 \sigma \sqrt{\mu_0/\epsilon_0} \left\{ \left[ |e_q^-|^2 + |e_q^+|^2 \right] \frac{\sinh(\kappa_i T)}{\kappa_i} + 2 \text{Re} \left[ e_q^- e_q^+ * (\hat{q}_\epsilon^- \cdot \hat{q}_\epsilon^+ *) \frac{\sin(\kappa_r T)}{\kappa_r} \right] \right\} \quad (49)$$

where  $S_0$  is the cross sectional area of the disk and  $q \in \{h, v\}$ . The  $e_q^\pm$  are given in Equations 18a,b,



and  $\kappa_r = \text{Re}(nk_0 K'_z)$ ,  $\kappa_i = \text{Im}(nk_0 K'_z)$  where  $K'_z$  is given by Equation 33c.

An analytical and a numerical method has been used to check that the solution given by Equation 25 does satisfy the optical theorem when  $ka \gg 1$ . The analytical check is made by asymptotically evaluating the integral for  $\sigma_s$  given by Equation 48a for  $ka \gg 1$ . This evaluation is carried out in Appendix D where an explicit formula for  $\sigma_s$  is given by Equation 6D. When this expression is used in the optical theorem along with Equation 49 and Equation 25, the conservation theorem has been shown to be satisfied identically.

Following the analytical check, a numerical check was made by computing  $\sigma_s$  and  $\sigma_a$  from Equations 48 and 49 and comparing their sum with the right hand side of Equation 47. Calculation were made for the case of a circular disk of radius 7cm, thickness 1mm and relative dielectric constant  $\tilde{\epsilon}_r = 36 + j13$ . The dielectric constant of the disk was chosen using the de Loor formula (Fung and Ulaby, 1978; de Loor, 1968) for leaves with 70% water at a frequency of 7 GHz. Two expressions for the total cross section were developed: The first,  $\sigma_T$ , was found by computing  $\sigma_a$  and  $\sigma_s$  from Equation 48 and 49. The second,  $\sigma'_T$ , was obtained by taking the imaginary part of  $4\pi (\hat{q} \cdot \overline{\hat{f}}(\hat{i}, \hat{i}) \cdot \hat{q}) / k_0$ . If the optical theorem is satisfied exactly then  $\sigma_T = \sigma'_T$ . The results of these calculations are shown in Tables I and II. Table I shows the results for a horizontally polarized wave incident at  $30^\circ$  with respect to the normal to the disk and Table II shows the results for a vertically polarized wave also incident at  $30^\circ$ . The tables list  $\sigma_s, \sigma_a, \sigma_T = \sigma_s + \sigma_a$  and the albedo,  $\sigma_s / \sigma_T$  all obtained numerically from Equations 48 and  $\sigma'_T$  obtained from Equations 47. Examples are shown in each table for frequencies of 1 GHz, 4 GHz and 7 GHz corresponding to  $ka$  of about 1.5, 5.0 and 10.3 respectively, since the theory is a high frequency theory valid for large  $ka$ , one expects energy conservation to be satisfied best for large  $ka$ . The results indicate agreement which improves with increasing  $ka$  and is within about 2% at the largest value of  $ka$ . To obtain the numerical results for scattering cross section the integrand,  $|\overline{\hat{f}}(\hat{i}, \hat{o}) \cdot \hat{q}|^2$  in the expression for  $\sigma_s$  has to be computed on a unit sphere. The results shown in Tables I and II were the result of computations using a grid of equally spaced points separated about  $3^\circ$  in  $\theta$  and  $\phi$ .

TABLE I (Horizontal Polarization)

frequency	$\sigma_s$	$\sigma_a$	$\sigma_T = \sigma_s + \sigma_a$	Albedo $\sigma_s/\sigma_T$	$\sigma'_T = \frac{4\pi}{k_0} \text{Im} [\hat{h} \cdot \bar{r}(\hat{i}, \hat{i}) \cdot \hat{h}]$	Error (%) $\frac{\sigma'_T - \sigma_T}{\sigma_T} \cdot 100$
1 GHz	.00147	.00276	0.00423	.23185	.00632	33.1%
4 GHz	.01465	.00318	0.01783	.79119	.01852	3.7%
7 GHz	.01908	.00264	0.02172	.86701	.02201	1.3%

TABLE II (Vertical Polarization)

frequency	$\sigma_s$	$\sigma_a$	$\sigma_T = \sigma_s + \sigma_a$	Albedo $\sigma_s/\sigma_T$	$\sigma'_T = \frac{4\pi}{k_0} \text{Im} [\hat{v} \cdot \bar{r}(\hat{i}, \hat{i}) \cdot \hat{v}]$	Error (%) $\frac{\sigma'_T - \sigma_T}{\sigma_T} \cdot 100$
1 GHz	.00121	.00233	.00354	.26354	.00458	22.8%
4 GHz	.01149	.00349	.01498	.71490	.01607	6.8%
7 GHz	.01676	.00315	.01991	.81966	.02045	2.6%

APPENDIX A

Polarization Vectors inside the Slab

The propagation vector  $\bar{K}_{\pm}$  for waves inside the slab can be obtained from the boundary conditions (Snell's law) at the surface of the disk. To do so, adopt the following notation in the reference frame of the disk:

$$\bar{K}_{\pm} = n k_0 [K_x^{\pm} \hat{x}' + K_y^{\pm} \hat{y}' + K_z^{\pm} \hat{z}'] = n k_0 \hat{K}^{\pm} \quad A1$$

$$\bar{i} = k_0 [i_x' \hat{x}' + i_y' \hat{y}' + i_z' \hat{z}'] = k_0 \hat{i} \quad A2$$

Since the boundary conditions must be satisfied for all  $x'$ ,  $y'$ , one has:

$$k_0 i_x' = n k_0 K_x^{\pm} \hat{\Delta} \triangleq n k_0 K_x' \quad A3$$

$$k_0 i_y' = n k_0 K_y^{\pm} \hat{\Delta} \triangleq n k_0 K_y' \quad A4$$

and since by definition the waves in the slab are propagating in opposite directions along the  $z'$ -axis, it follows that:

$$\bar{K}_{\pm} = n k_0 [K_x' \hat{x}' + K_y' \hat{y}' \pm K_z' \hat{z}'] \quad A5$$

Now using  $\bar{K}_{\pm} \cdot \bar{K}_{\pm} = (n k_0)^2$  which follows from the wave equation, one can solve for  $K_z'$ :

$$\begin{aligned} K_z' &= \frac{1}{n k_0} \sqrt{(n k_0)^2 [1 - (K_x')^2 - (K_y')^2]} \\ &= \frac{1}{n k_0} \sqrt{(n k_0)^2 - k_0^2 [(i_x')^2 + (i_y')^2]} \\ &= \frac{1}{n} \sqrt{(n^2 - 1) + (i_z')^2} \\ &= \frac{1}{n} \sqrt{(n^2 - 1) + (\hat{i} \cdot \hat{n})^2} \end{aligned} \quad A6$$

Now using Equations A3, A4 and A6 in Equation A5 one can obtain an expression for  $\bar{K}_{\pm}$ :

$$\begin{aligned} \bar{K}_{\pm} &= k_0 [i_x' \hat{x}' + i_y' \hat{y}'] \pm n k_0 \left[ \frac{1}{n} \sqrt{(n^2 - 1) + (\hat{i} \cdot \hat{n})^2} \right] \hat{n} \\ &= k_0 \left\{ [\hat{i} - (\hat{i} \cdot \hat{n}) \hat{n}] \pm \sqrt{(n^2 - 1) + (\hat{i} \cdot \hat{n})^2} \hat{n} \right\} \\ &= k_0 \left\{ \hat{i} + \Omega_{\pm} \hat{n} \right\} \end{aligned} \quad A7$$

where

$$\Omega_{\pm} = -(\hat{i} \cdot \hat{n}) \pm \sqrt{(n^2 - 1) + (\hat{i} \cdot \hat{n})^2} \quad A8$$

Thus

$$\hat{K}_{\pm} = \frac{1}{n k_0} \bar{K}_{\pm} = \frac{1}{n} [i + \Omega_{\pm} \hat{n}] \quad \text{A9}$$

This result can now be used to obtain an expression for the unit vectors in the direction of horizontal and vertical polarization inside the disk. One obtains:

$$\hat{h}_{\epsilon}^{\pm} = \frac{\hat{K}_{\pm} \times \hat{n}}{|\hat{K}_{\pm} \times \hat{n}|} = \frac{i \times \hat{n}}{|i \times \hat{n}|} \triangleq \hat{h} \quad \text{A10}$$

$$\hat{v}_{\epsilon}^{\pm} = \hat{h}_{\epsilon}^{\pm} \times \hat{K}_{\pm} = \hat{h} \times \hat{K}_{\pm} = \frac{1}{n} [\hat{v} + \Omega_{\pm} \hat{h} \times \hat{n}] \quad \text{A11}$$

Notice that although  $\hat{h}_{\epsilon}^{+} = \hat{h}_{\epsilon}^{-} = \hat{h}$  the unit vectors of the vertically polarized waves in the slab in general are not in the same direction:  $\hat{v}_{\epsilon}^{+} \neq \hat{v}_{\epsilon}^{-}$ . This is true because the two waves inside the slab do not propagate in the same direction. This is illustrated in Figure 16. At normal incidence  $\hat{v}_{\epsilon}^{+} = -\hat{v}_{\epsilon}^{-} = -\hat{v}$ .

## APPENDIX B

### Euler Angles for Orientation of the Disk

The Euler angles which specify the orientation of the disk consist of three coordinate rotations. Starting with the reference coordinate system and coordinate system for the disk aligned, one performs the following counterclockwise rotations:

1. Rotate  $\phi$  degrees about the original  $z = z'$  axis

$$\begin{bmatrix} x' \\ y' \\ z' \end{bmatrix} = \begin{bmatrix} \cos\phi & \sin\phi & 0 \\ -\sin\phi & \cos\phi & 0 \\ 0 & 0 & 1 \end{bmatrix} \begin{bmatrix} x \\ y \\ z \end{bmatrix}$$

2. Next rotate  $\theta$  degrees about the new x-axis

$$\begin{bmatrix} x'' \\ y'' \\ z'' \end{bmatrix} = \begin{bmatrix} 1 & 0 & 0 \\ 0 & \cos\theta & \sin\theta \\ 0 & -\sin\theta & \cos\theta \end{bmatrix} \begin{bmatrix} x' \\ y' \\ z' \end{bmatrix}$$

3. Finally rotate  $\gamma$  degrees about the new z-axis

$$\begin{bmatrix} x''' \\ y''' \\ z''' \end{bmatrix} = \begin{bmatrix} \cos\gamma & \sin\gamma & 0 \\ -\sin\gamma & \cos\gamma & 0 \\ 0 & 0 & 1 \end{bmatrix} \begin{bmatrix} x'' \\ y'' \\ z'' \end{bmatrix}$$

These three rotations are applied in succession to obtain the relationship between the reference coordinate system  $(x,y,z)$  and the final coordinate system fixed on the disk  $(x',y',z')$ . Thus:

$$\begin{bmatrix} x' \\ y' \\ z' \end{bmatrix} = \begin{bmatrix} \cos\gamma & \sin\gamma & 0 \\ -\sin\gamma & \cos\gamma & 0 \\ 0 & 0 & 1 \end{bmatrix} \begin{bmatrix} 1 & 0 & 0 \\ 0 & \cos\theta & \sin\theta \\ 0 & -\sin\theta & \cos\theta \end{bmatrix} \begin{bmatrix} \cos\phi & \sin\phi & 0 \\ -\sin\phi & \cos\phi & 0 \\ 0 & 0 & 1 \end{bmatrix} \begin{bmatrix} x \\ y \\ z \end{bmatrix}$$

or

$$\begin{aligned} x' &= [\cos\gamma\cos\phi - \sin\gamma\sin\phi\cos\theta] x + [\cos\gamma\sin\phi + \sin\gamma\cos\phi\cos\theta] y + [\sin\theta\sin\gamma] z \\ y' &= -[\sin\gamma\cos\phi + \cos\gamma\sin\phi\cos\theta] x + [-\sin\gamma\sin\phi + \cos\gamma\cos\phi\cos\theta] y + [\sin\theta\cos\gamma] z \\ z' &= [\sin\theta\sin\phi] x + [-\sin\theta\cos\phi] y + [\cos\theta] z \end{aligned}$$

## APPENDIX C

### The Shape Function $\tilde{S}(\nu'_t)$

The shape function  $\tilde{S}(\nu'_t)$  is defined in the reference frame of the slab by

$$\tilde{S}(\nu'_t) = \iint S(\bar{r}'_t) e^{-j2\pi\nu'_t \cdot \bar{r}'_t} d\bar{r}'_t$$

where  $S(\bar{r}'_t)$  is the cross sectional shape of the disk and where

$$\nu'_t = \frac{k_0}{2\pi} [\hat{i}'_t - \hat{o}'_t] = \frac{k_0}{2\pi} \hat{n} \times [(\hat{i} - \hat{o}) \times \hat{n}]$$

$$\bar{r}'_t = x' \hat{x} + y' \hat{y}$$

It is necessary to express this function in the coordinates of the reference frame (but the integration is done in the primed coordinate system.) The problem is to express  $\nu'_t$  in terms of the reference coordinates (angles  $\theta_i, \phi_i$  and  $\theta_s, \phi_s$  and  $\theta, \phi, \gamma$ ). Since  $\nu'_x$  and  $\nu'_y$  are the projections of  $\nu'_t$  on the  $x'$  and  $y'$  axes and since dot (scalar) products are invariant under coordinate rotations, one can write

$$\nu'_x = \frac{k_0}{2\pi} (\hat{i} - \hat{o}) \cdot \hat{x}'$$

$$\nu'_y = \frac{k_0}{2\pi} (\hat{i} - \hat{o}) \cdot \hat{y}'$$

where  $\hat{i}, \hat{o}$  are the directions of propagation of the incident and scattered waves as seen in the reference coordinate frames:

$$\hat{i} = -\sin\theta_i [\cos\phi_i \hat{x} + \sin\phi_i \hat{y}] - \cos\theta_i \hat{z}$$

$$\hat{o} = \sin\theta_s [\cos\phi_s \hat{x} + \sin\phi_s \hat{y}] + \cos\theta_s \hat{z}$$

and  $\hat{x}', \hat{y}'$  are unit vectors along the  $x$  and  $y$  axes of the disk but as seen by an observer in the reference system. These unit vectors can be obtained from the Euler angle rotations (Appendix B):

$$\hat{x}' = [\cos\gamma \cos\phi - \sin\gamma \sin\phi \cos\theta] \hat{x} +$$

$$+ [\cos\gamma \sin\phi + \sin\gamma \cos\phi \cos\theta] \hat{y} + \sin\theta \sin\gamma \hat{z}$$

$$\hat{y}' = -[\sin\gamma \cos\phi + \cos\gamma \sin\phi \cos\theta] \hat{x} +$$

$$+ [-\sin\gamma \sin\phi + \cos\gamma \cos\phi \cos\theta] \hat{y} + \sin\theta \cos\gamma \hat{z}$$

$$\hat{z}' = \sin\theta [\sin\phi \hat{x} - \cos\phi \hat{y}] + \cos\theta \hat{z}$$

from which one obtains

$$\nu'_x = \frac{k_0}{2\pi} [\alpha \sin\gamma - \beta \cos\gamma]$$

$$\nu'_y = \frac{k_0}{2\pi} [\beta \sin\gamma + \alpha \cos\gamma]$$

where

$$\alpha = \cos\theta [\sin\theta_i \sin(\phi - \phi_i) + \sin\theta_s \sin(\phi - \phi_s)] - \sin\theta [\cos\theta_i + \cos\theta_s]$$

$$\beta = \sin\theta_i \cos(\phi - \phi_i) + \sin\theta_s \cos(\phi - \phi_s)$$

An important special case is that of a circular disk of radius  $a$ . By changing variables so that the integration can be done in cylindrical coordinates one obtains:

$$\tilde{\mathfrak{S}}(\nu') = \frac{a}{\nu} J_1(2\pi\nu a)$$

where

$$\nu = \frac{k_0}{2\pi} \sqrt{\alpha^2 + \beta^2}$$

and  $J_1(x)$  is a Bessel function of first kind of order unity.

## APPENDIX D

### High Frequency Evaluation of $\sigma_s$

The scattering cross section,  $\sigma_s$ , is evaluated asymptotically for large  $k_0 a$  in this appendix. Starting with the definition of scattering cross section (Equation 48a) and using Equation 25 for  $\bar{f}(\hat{i}, \hat{o})$  on obtains:

$$\sigma_s = C \int_{\text{sphere}} \int |\tilde{S}(\vec{v}'_t)|^2 W^{(q)}(\theta, \phi) d\Omega \quad 1-D$$

where

$$W^{(q)}(\theta, \phi) = |\bar{F}(\hat{i}, \hat{o}) \cdot \hat{q}|^2 = |\text{sinc}(\theta^+) \epsilon_q^+ \hat{q}_\epsilon^+ + \text{sinc}(\theta^-) \epsilon_q^- \hat{q}_\epsilon^-|^2 \quad 2-D$$

$$\theta^\pm = \frac{1}{2} k_0 T [nK'_z \pm \alpha'_z] \quad 3-D$$

$$C = \left| \frac{\tilde{\chi}_a}{4\pi} k_0^2 T \right|^2 \quad 4-D$$

and  $q \in \{h, v\}$  and the subscript "e" in Equation 2-D indicates polarization unit vectors of waves inside the disk (see Equations 29-31). Without loss of generality, it has been assumed that the disc remains in its unrotated position ( $\theta = \phi = \gamma = 0$ ).

When  $k_0 a \gg 1$ , the function  $|\tilde{S}(\vec{v}'_t)|^2$  appearing in Equation 1-D becomes very sharply peaked at the angle of reflection ( $\theta_r, \phi_r$ ) and the angle of transmission ( $\theta_t, \phi_t$ ); and since  $W^{(q)}(\theta, \phi)$  is a smoothly varying function under most conditions, the major contribution to  $\sigma_s$  for large  $k_0 a$  is expected to come from the vicinity of specular reflection and transmission. This leads to a procedure to evaluate the integral in Equation 1-D which is asymptotically correct for large  $k_0 a$ . To formally carry out the procedure, the integral over the spherical surface surrounding the disk is projected onto two integrals in the plane of the disc by means of the transformation.

$$\begin{aligned} \alpha_x &= \sin\theta \cos\phi \\ \alpha_y &= \sin\theta \sin\phi \end{aligned} \quad 5-D$$



The transformed expression is:

$$\sigma_s = C \left\{ \int_{A_r} + \int_{A_t} \right\} |\tilde{S}(\vec{v}')|^2 W^{(q)}(\theta, \phi) \frac{d\alpha_x d\alpha_y}{|\cos \theta|}$$

where

6-D

$$A_{r,t} = \left\{ \alpha_x^2 + \alpha_y^2 \leq 1, \cos \theta \geq 0 \right\}$$

Using the sharply peaked character of  $|\tilde{S}(\vec{v}')|^2$ , Equation 6D becomes

$$\sigma_s = \frac{CW^{(q)}(\theta_r, \phi_r)}{|\cos \theta_r|} \int_{A_r} |\tilde{S}(\vec{v}')|^2 d\alpha_x d\alpha_y + \frac{CW^{(q)}(\theta_t, \phi_t)}{|\cos \theta_t|} \int_{A_t} |\tilde{S}(\vec{v}')|^2 d\alpha_x d\alpha_y \quad 7-D$$

Once again using the fact that  $k_0 a \gg 1$ , the integrals in Equation 7D can be extended to the whole  $\alpha_x, \alpha_y$  plane. The resulting integrals can then be evaluated exactly by employing Equation 22c.

The result is

$$\sigma_s = \frac{(2\pi)^2 CS_0}{k_0 \cos \theta_i} [W^{(q)}(\theta_r, \phi_r) + W^{(q)}(\theta_t, \phi_t)] \quad 8-D$$

where  $S_0$  is the area of the disc. In arriving at Equation 6D the identity  $\cos \theta_i = |\cos \theta_r| = |\cos \theta_t|$  has been used.

## REFERENCES

- Andrejewski, W. (1952), "Die Beugung Elektromagnetischer Wellen an der leitenden Kreisscheibe und an der kreisformigen Öffnung im leitenden ebenen Schirm", dissertation for Rheinisch-Wesfälischen Technischen Hochschule, Aachen, Germany.
- Born, M and E. Wolf (1959), *Principles of Optics*, Pergamon Press, Section 3.5
- Bowman, J. J., T. B. A. Senior and P. L. E. Uslengi, Editors, (1969), *Electromagnetic and Acoustic Scattering by Simple Shapes*, North-Holland, Chapter 14 (by F. B. Sleator)
- de Loor, G. P. (1968), "Dielectric Properties of Heterogeneous Mixtures Containing Water", J. Microwave Power, Vol. 3, pp 67-73.
- Fung, A. and F. Ulaby (1978), "A Scatter Model for Leafy Vegetation", IEEE Trans. Geosci. Electronics, Vol 16 (#4), pp 281-286
- Goldstein, J. (1966), *Classical Mechanics*, Addison-Wesley, Chapter 4.
- Hodge, D. B. (1980), "Scattering by Circular Metal Disks", IEEE trans. on Antennas and Propagation, Vol. AP-28 (#5), pp. 707-712.
- Lang, R. H. (1981), "Electromagnetic Backscattering from a Sparse Distribution of Lossy Dielectric Scatterers", Radio Science, Vol 16 (#1), pp 15 - 30.
- Meixner, J. and W. Andrejewski (1950), "Strenge Theorie der Beugung ebener electromagnetischer Wellen an der vollkommen leitenden Kreisscheibe und an der kreisformigen Öffnung im leitenden ebenen Schirm", Ann. Phys Vol. 7, pp 157
- Ruck, G. T., D. E. Barrick, W. D. Stuart and C. K. Krichbaum (1970), *Radar Cross Section Handbook*, Vol 2, Plenum Press, New York.

Schiffer, R. and K. O. Thielheim (1979), "Light Scattering by Dielectric Needles and Disks", J. Applied Physics, Vol 50 (#4), pp 2476-2483.

Weil, H. and C-M Chu (1976a), "Scattering and Absorption of Electromagnetic Radiation by Thin Dielectric Disks", Applied Optics, Vol 15 (#7), pp 1832-1836.

Weil, H. and C-M Chu (1976b), "Integral Equation Method for Scattering and Absorption of Electromagnetic Radiation by thin Lossy Dielectric Disks", J. Computational Phys., Vol 22 (#1), pp 111-124.

## FIGURE CAPTIONS

Figure 1. Problem Geometry.

Figure 2. Eulerian angles ( $\theta, \phi, \gamma$ ) which describe the disk orientation.

Figure 3. Geometry as seen in the coordinate frame fixed on the disk. The origin is half-way between the parallel faces of the disk.

Figure 4. Geometry used in calculating the examples.  $\theta_i = 30^\circ$  and  $\hat{i}$  is in the y-z plane.  $\hat{n}$  is also in the y-z plane and except where noted  $\hat{n} = \hat{z}$  as shown here.

Figure 5. Components of the scattering amplitude when the observer is in the plane of incidence ( $0^\circ$ ), perpendicular to the plane of incidence ( $90^\circ$ ) and half-way between ( $45^\circ$ ).

Figure 6. Magnitude of the scattering amplitude,  $f_{hh}$ , in the plane of incidence as a function of  $ka$ .

Figure 7. Magnitude of the scattering amplitude,  $f_{vv}$ , in the plane of incidence as a function of  $ka$ .

Figure 8. Magnitude of the scattering amplitude,  $f_{hh}$ , as a function of disk orientation.  $\theta$  is the angle between  $\hat{n}$  and  $\hat{i}$ .

Figure 9. Magnitude of the scattering amplitude,  $f_{vv}$ , as a function of disk orientation.  $\theta$  is the angle between  $\hat{n}$  and  $\hat{i}$ .

Figure 10. Magnitude of the scattering amplitude,  $f_{hh}$ , in the plane of incidence as a function of dielectric constant (no loss):  $\tilde{\epsilon}_r = \epsilon'$ .

Figure 11. Magnitude of the scattering amplitude,  $f_{vv}$ , in the plane of incidence as a function of dielectric constant (no loss):  $\tilde{\epsilon}_r = \epsilon'$ .

Figure 12. Magnitude of the scattering amplitude,  $f_{hh}$ , in the plane of incidence near resonance for dielectric with loss.

Figure 12. Magnitude of the scattering amplitude,  $f_{vv}$ , in the plane of incidence near resonance for dielectric with loss.

Figure 14. Magnitude of the scattering amplitude,  $f_{hh}$ , in the plane of incidence for purely lossy dielectric:  $\tilde{\epsilon}_r = j\epsilon''$ .

Figure 15. Magnitude of the scattering amplitude,  $f_{vv}$ , in the plane of incidence for purely lossy dielectric:  $\tilde{\epsilon}_r = j\epsilon''$ .

Figure 16. Polarization and propagation vectors inside the slab.

ORIGINAL PAGE IS  
OF POOR QUALITY

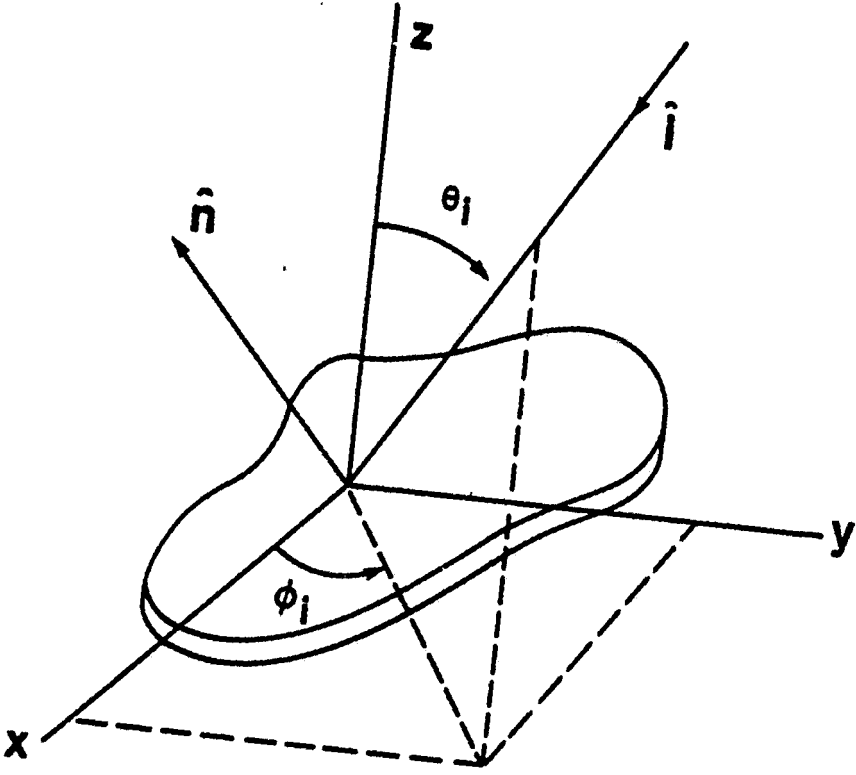


Figure 1. Problem Geometry.

ORIGINAL PAGE IS  
OF POOR QUALITY

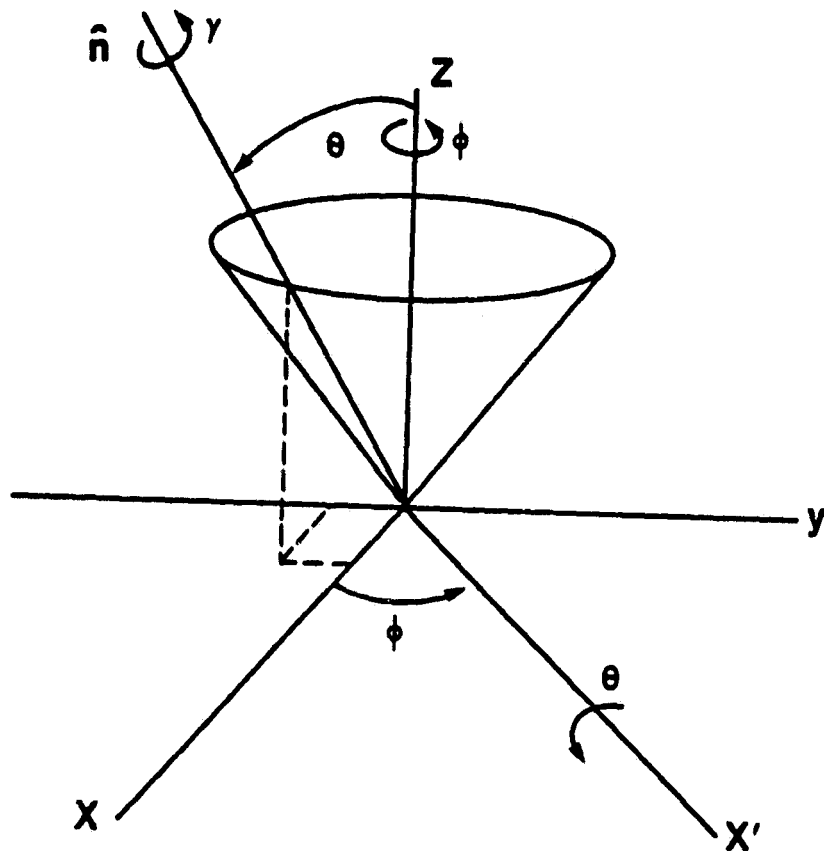


Figure 2. Eulerian angles ( $\theta$ ,  $\phi$ ,  $\gamma$ ) which describe the disk orientation.

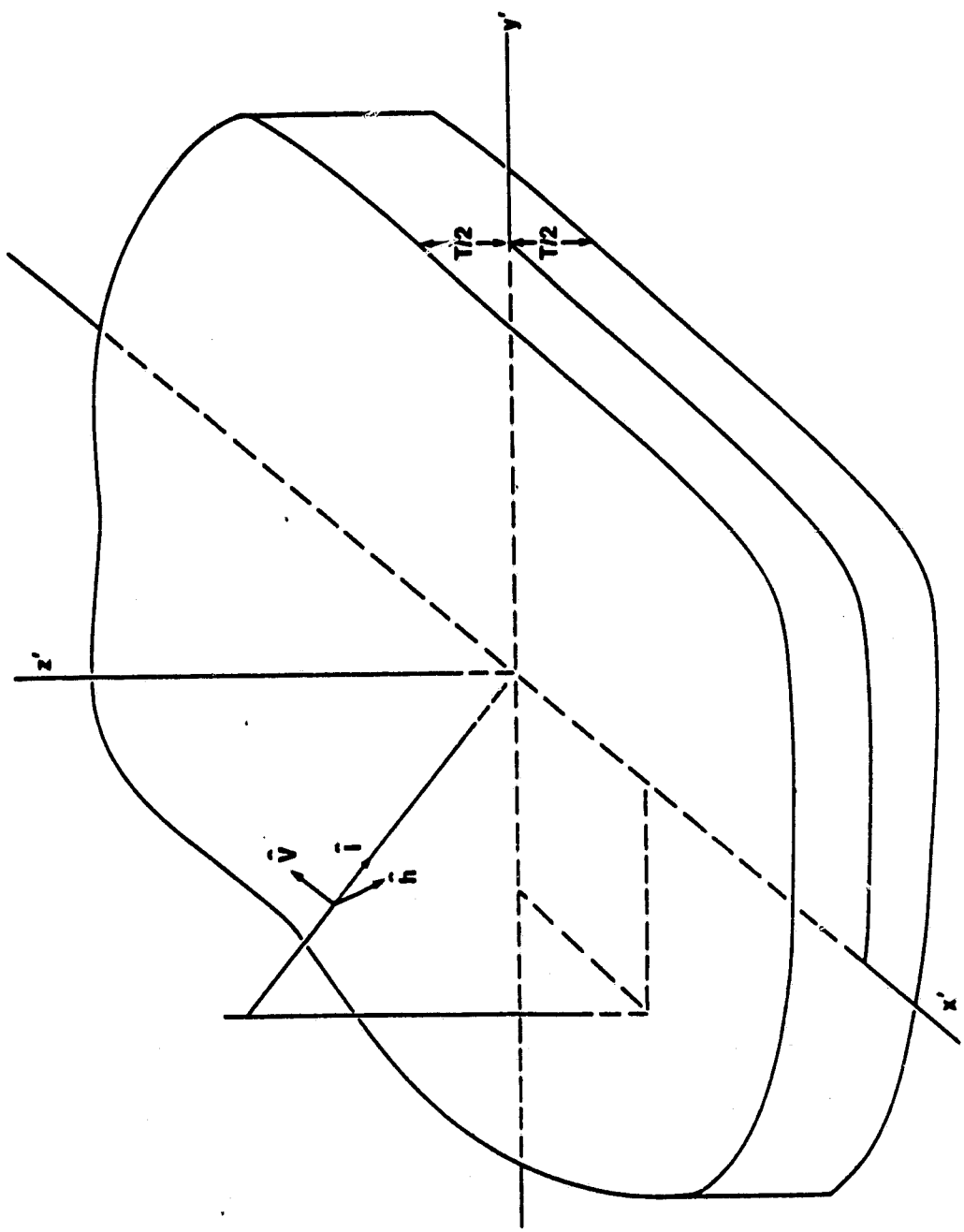


Figure 3. Geometry as seen in the coordinate frame fixed on the disk. The origin is half-way between the parallel faces of the disk.



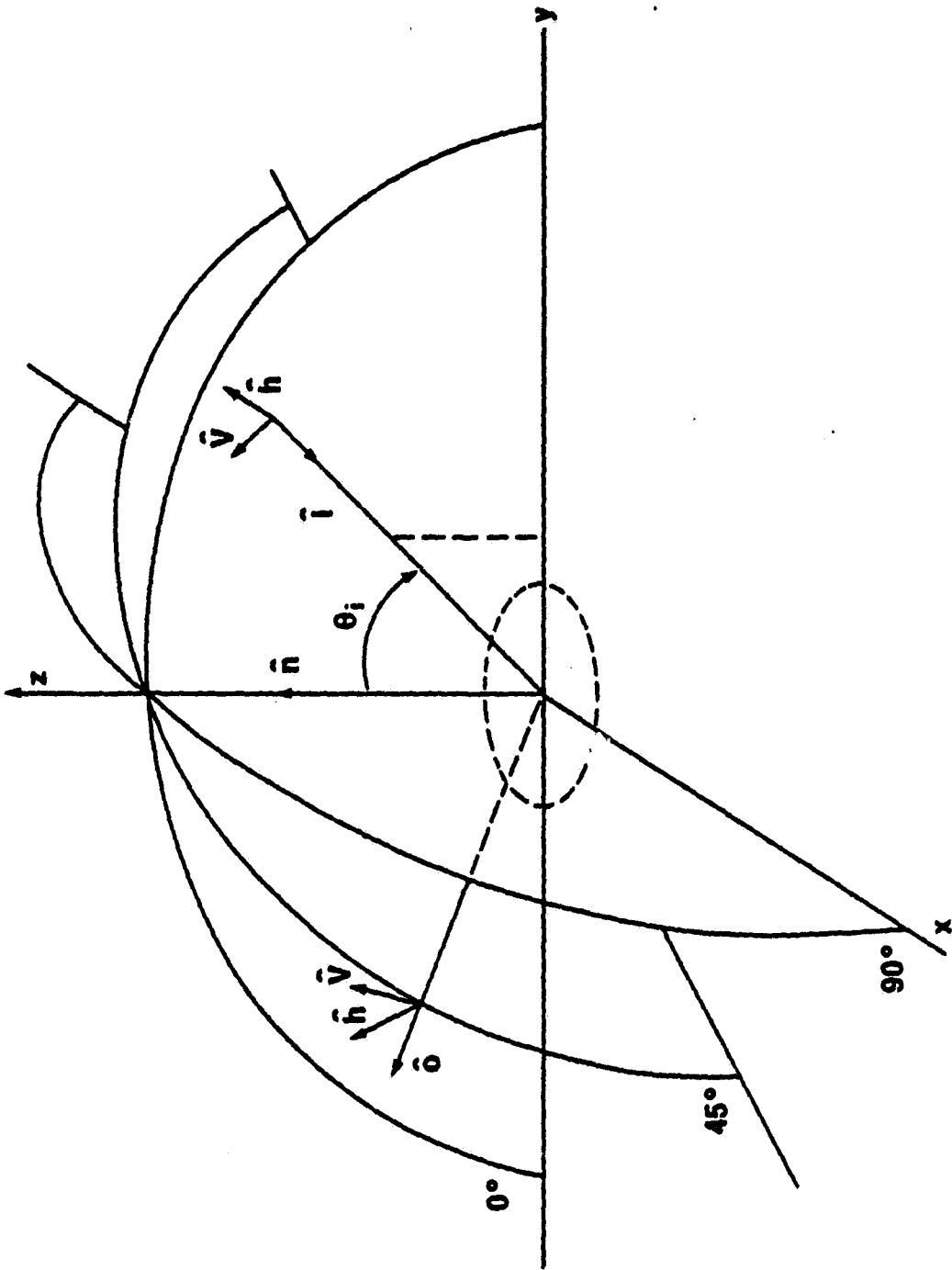


Figure 4. Geometry used in calculating the examples.  $\theta_i = 30^\circ$  and  $\hat{i}$  is in the  $y-z$  plane.  $\hat{n}$  is also in the  $y-z$  plane and except where noted  $\hat{n} = \hat{z}$  as shown here.

ORIGINAL PAGE IS  
OF POOR QUALITY

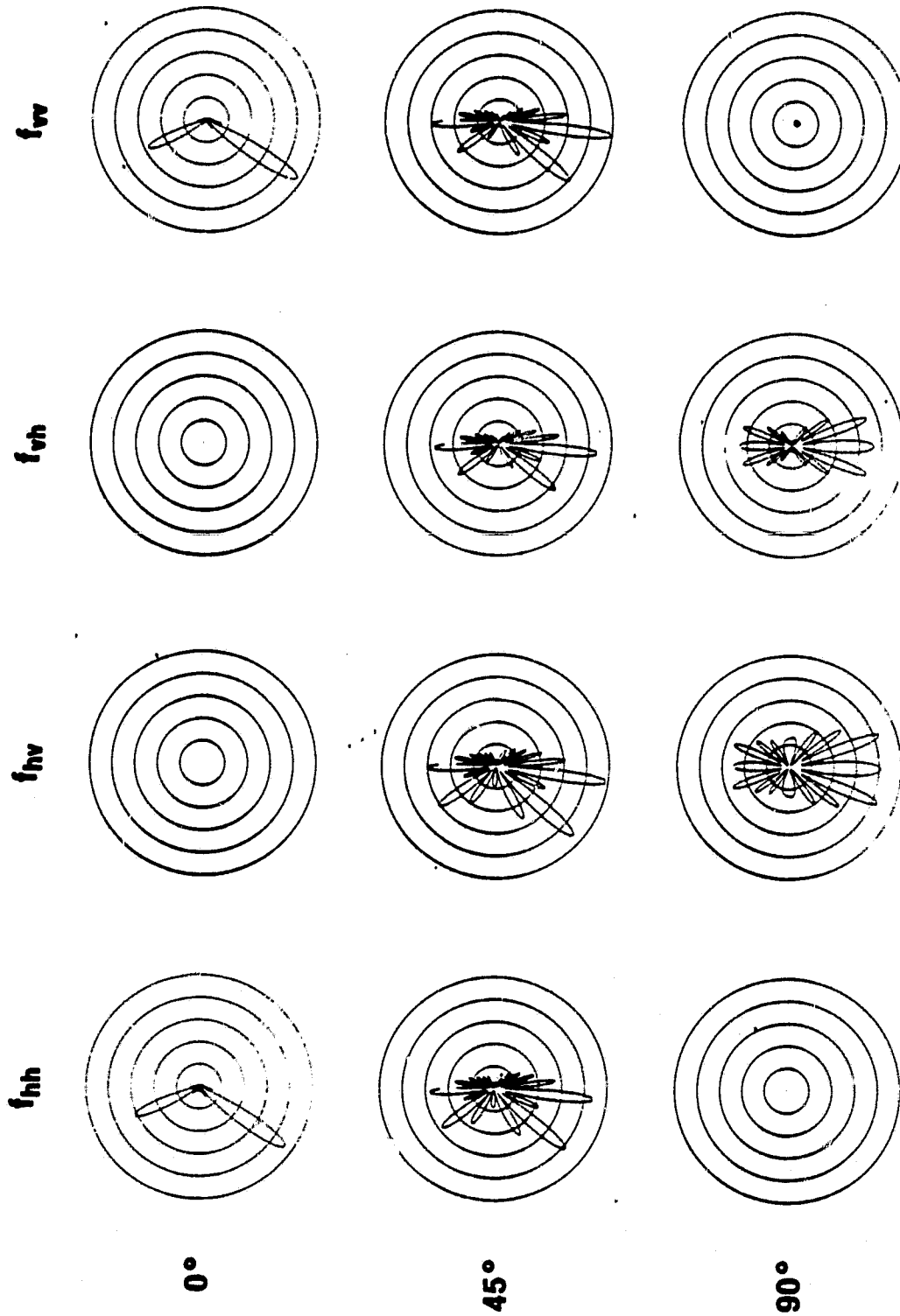


Figure 5. Components of the scattering amplitude when the observer is in the plane of incident ( $0^\circ$ ), perpendicular to the plane of incidence ( $90^\circ$ ) and half-way between ( $45^\circ$ ).

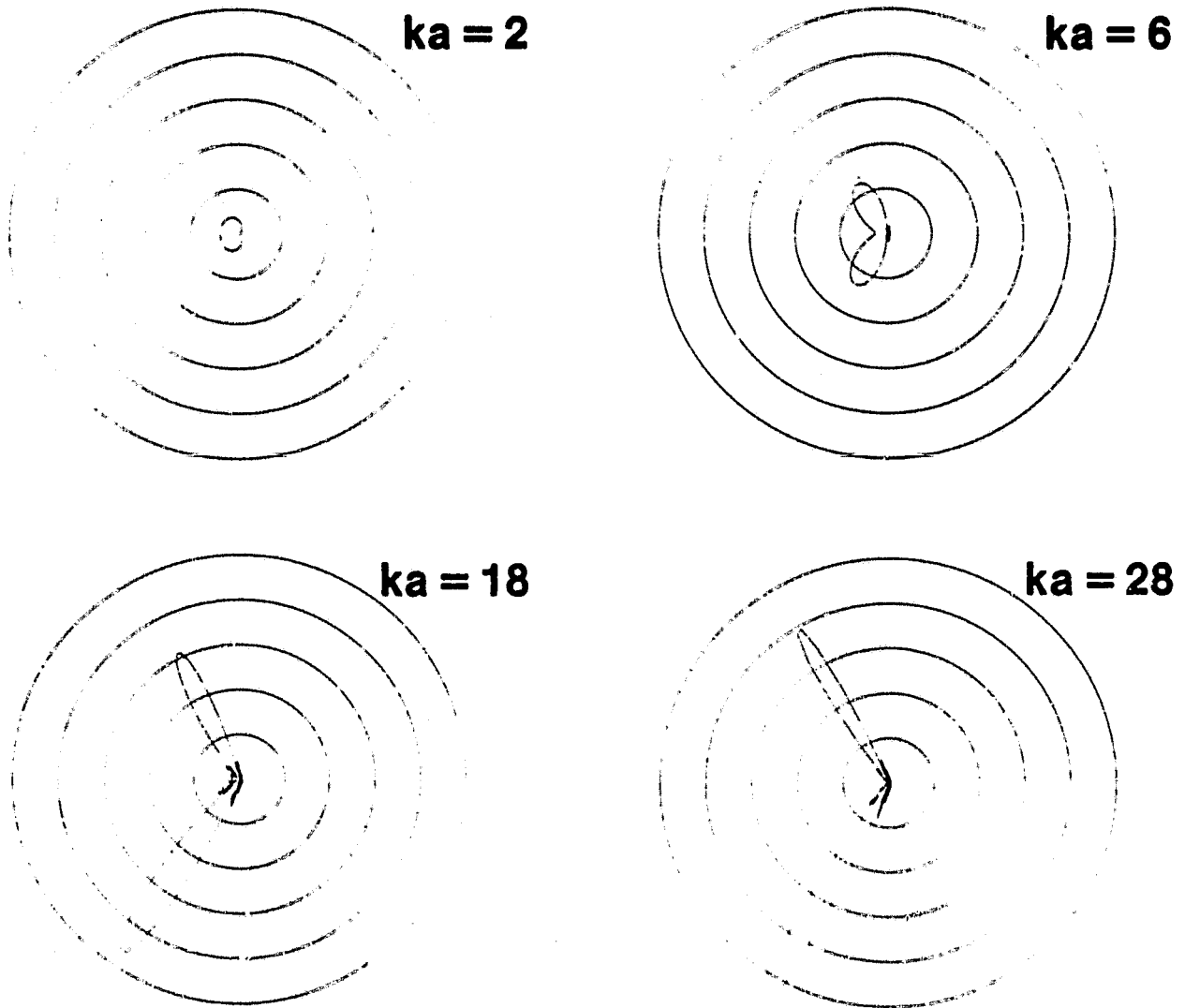


Figure 6. Magnitude of the scattering amplitude,  $f_{hh}$ , in the plane of incidence as a function of  $ka$ .

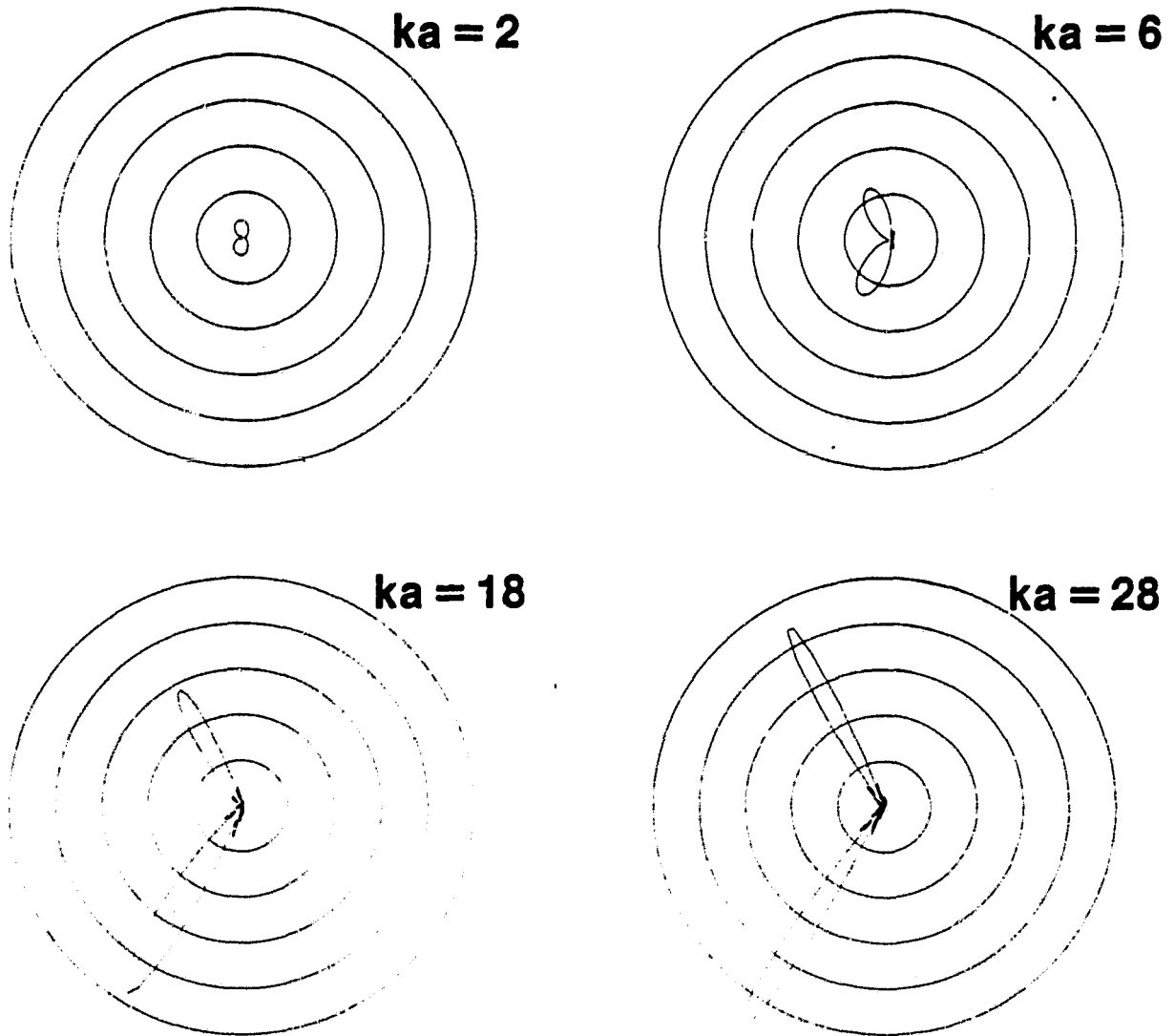


Figure 7. Magnitude of the scattering amplitude,  $f_w$ , in the plane of incidence as a function of  $ka$ .

ORIGINAL PAGE IS  
OF POOR QUALITY

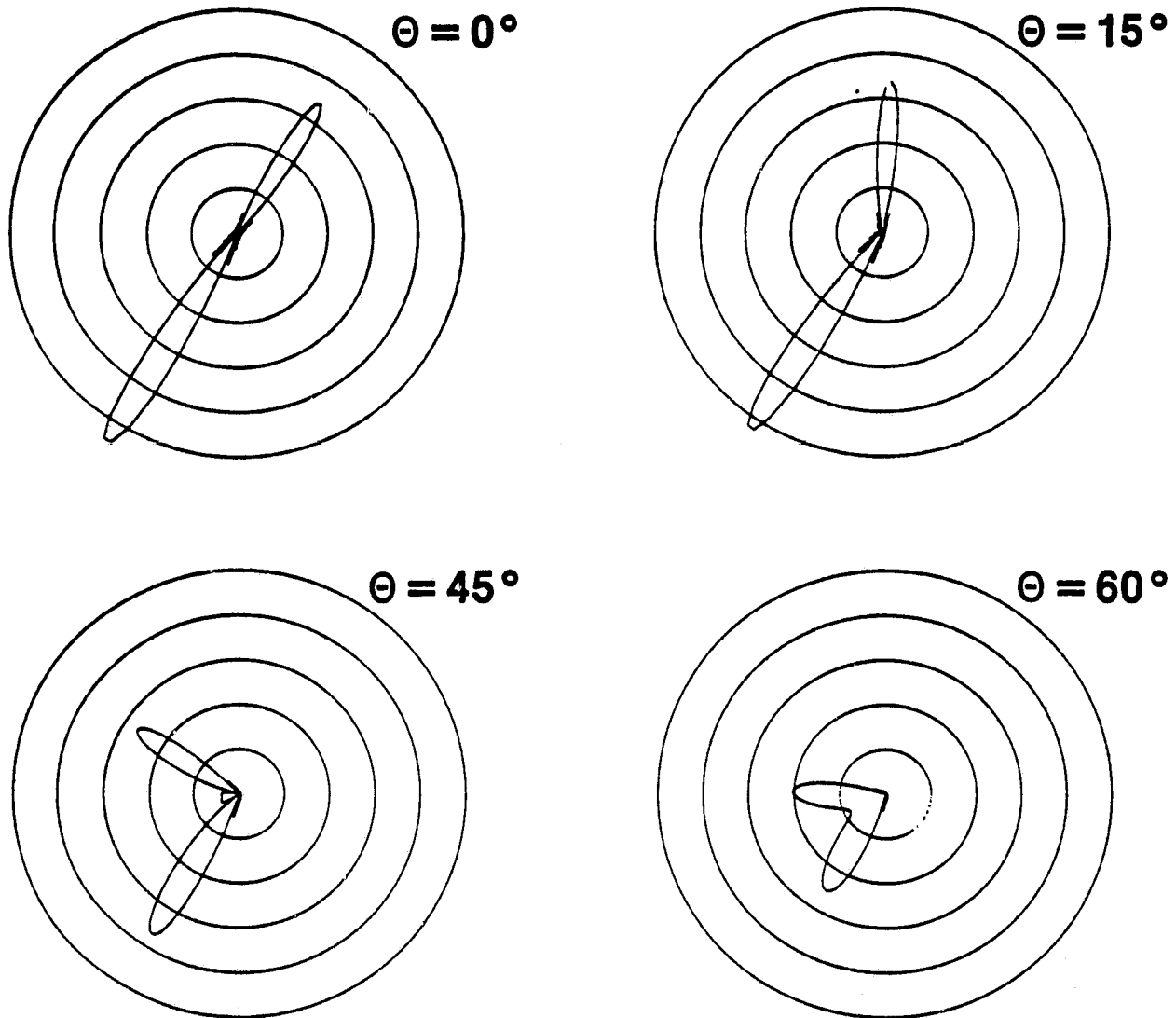


Figure 8. Magnitude of the scattering amplitude,  $f_{hh}$ , as a function of disk orientation.  $\theta$  is the angle between  $\hat{n}$  and  $\hat{i}$ .

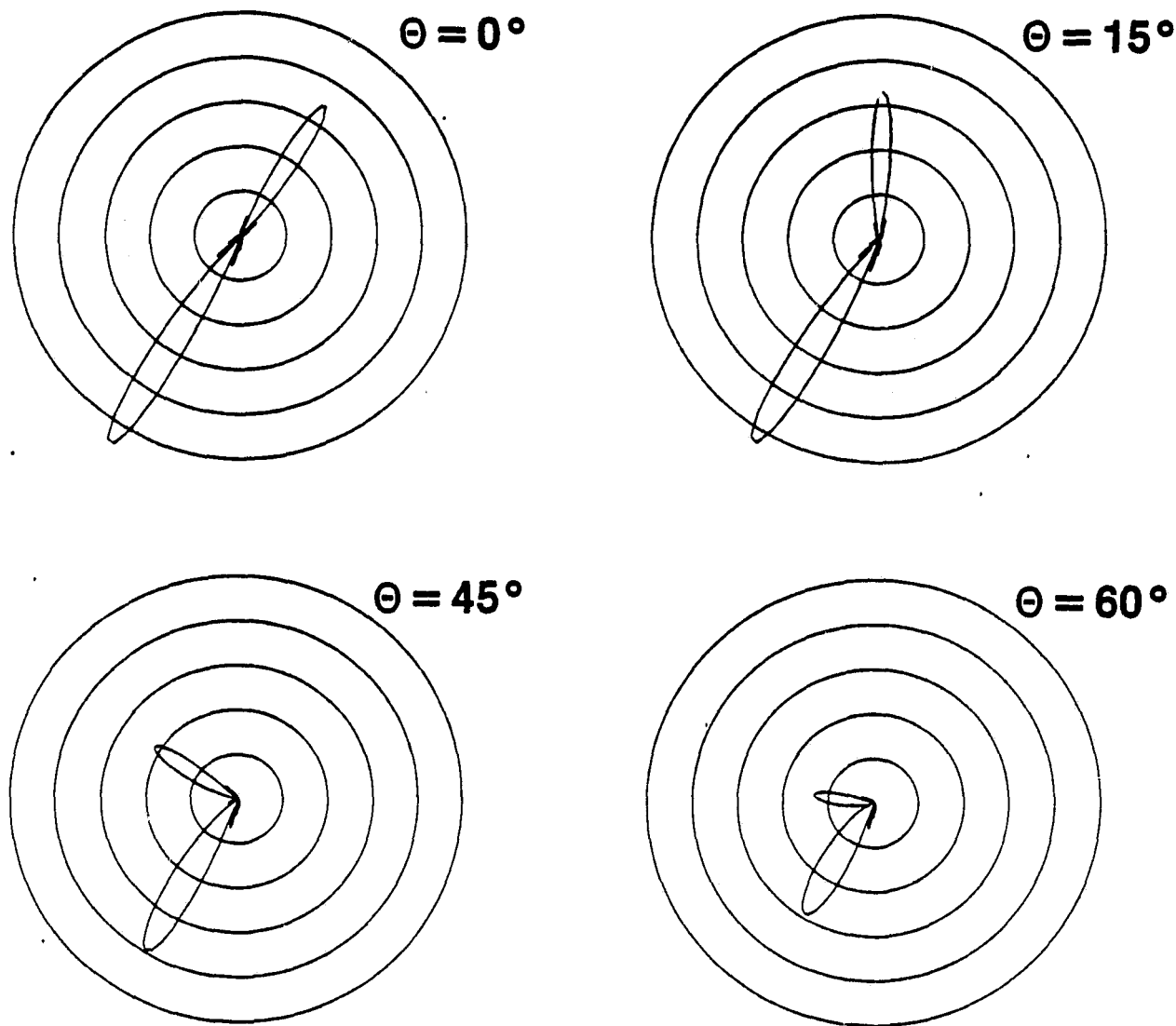


Figure 9. Magnitude of the scattering amplitude,  $f_w$ , as a function of disk orientation.  $\theta$  is the angle between  $\hat{n}$  and  $\hat{i}$ .

ORIGINAL PAGE IS  
OF POOR QUALITY

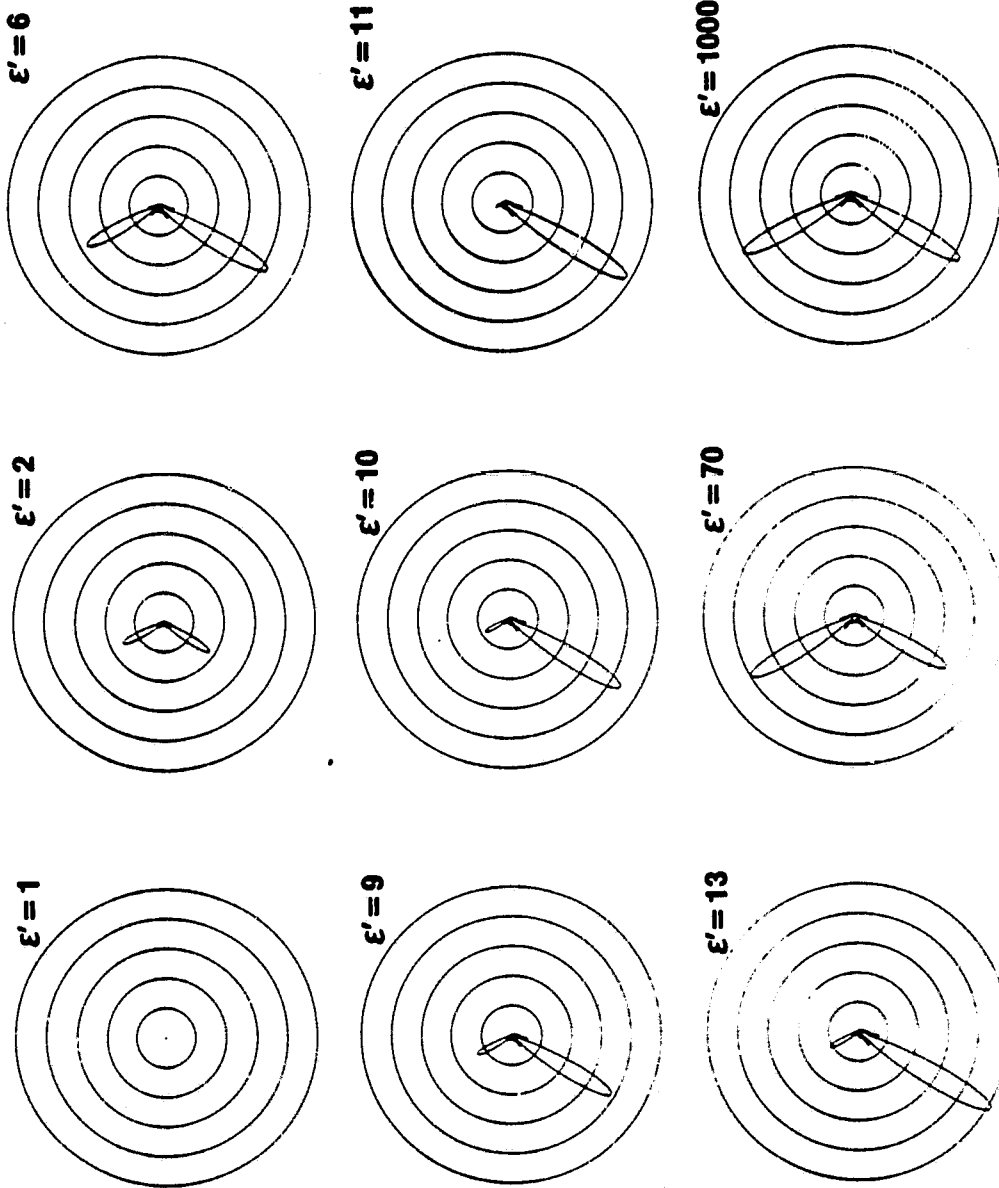


Figure 10. Magnitude of the scattering amplitude,  $f_{hh}$ , in the plane of incidence as a function dielectric constant (no loss):  $\tilde{\epsilon}_T = \epsilon'$ .

ORIGINAL PAGE IS  
OF POOR QUALITY

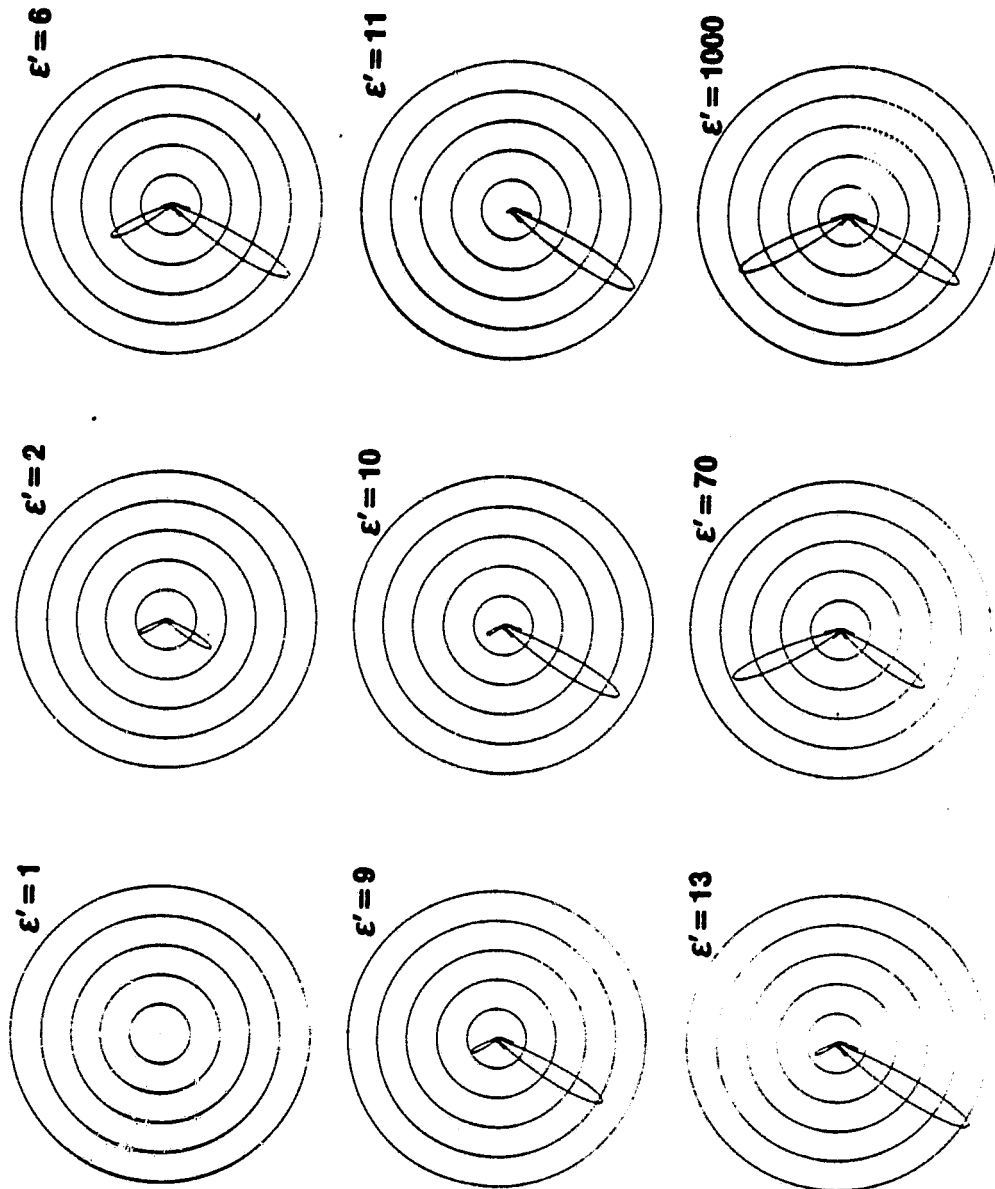


Figure 11. Magnitude of the scattering amplitude,  $f_w$ , in the plane of incidence as a function of dielectric constant (no loss):  $\tilde{\epsilon}_1 = \epsilon'$ .



ORIGINAL IMAGE IS  
OF POOR QUALITY

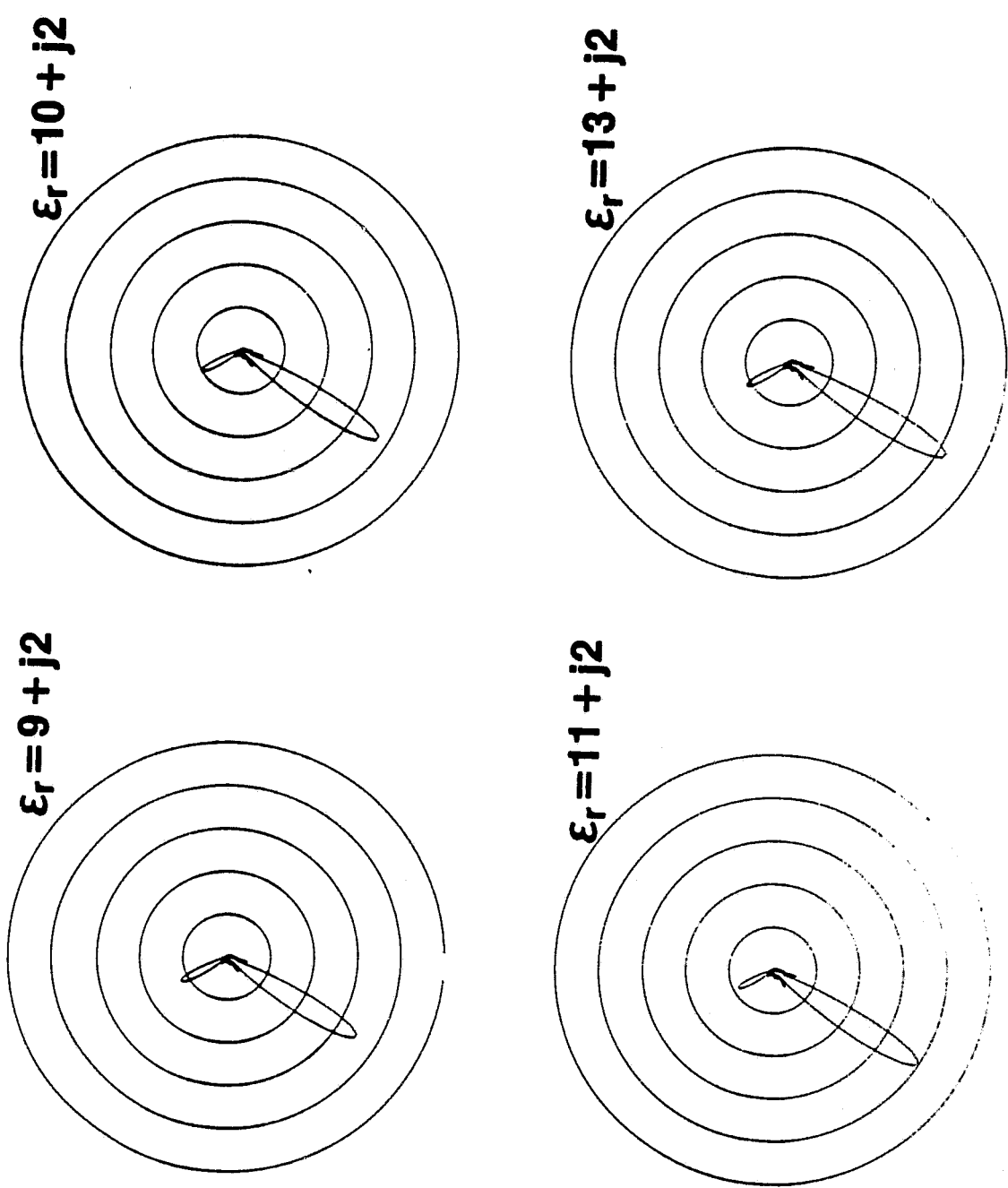


Figure 12. Magnitude of the scattering amplitude,  $f_{hh}$ , in the plane of incidence near resonance for dielectric with loss.

ORIGINAL PAGE IS  
OF POOR QUALITY.

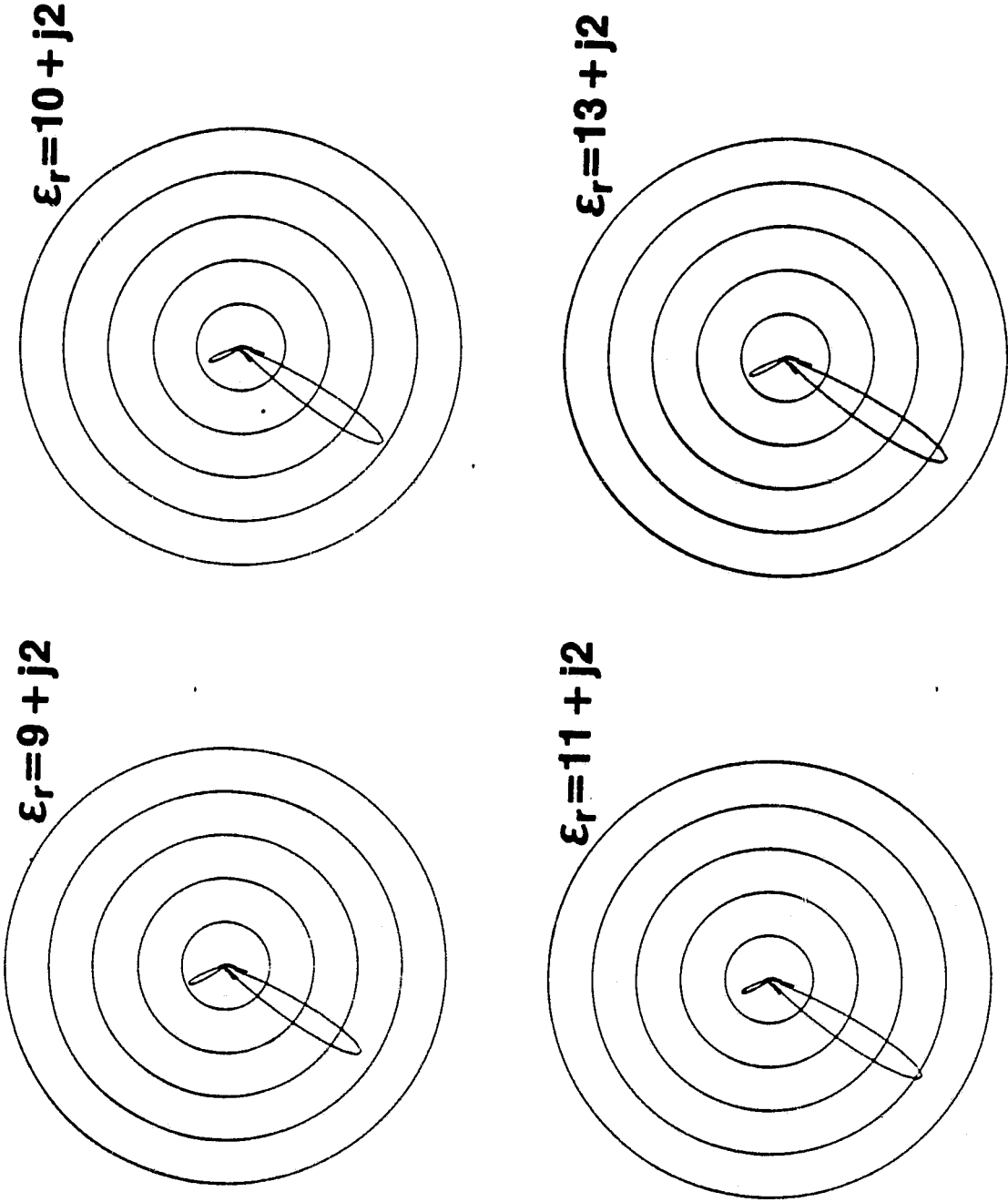


Figure 13. Magnitude of the scattering amplitude,  $f_w$ , in the plane of incidence near resonance for dielectric with loss.

ORIGINAL PAGE IS  
OF POOR QUALITY

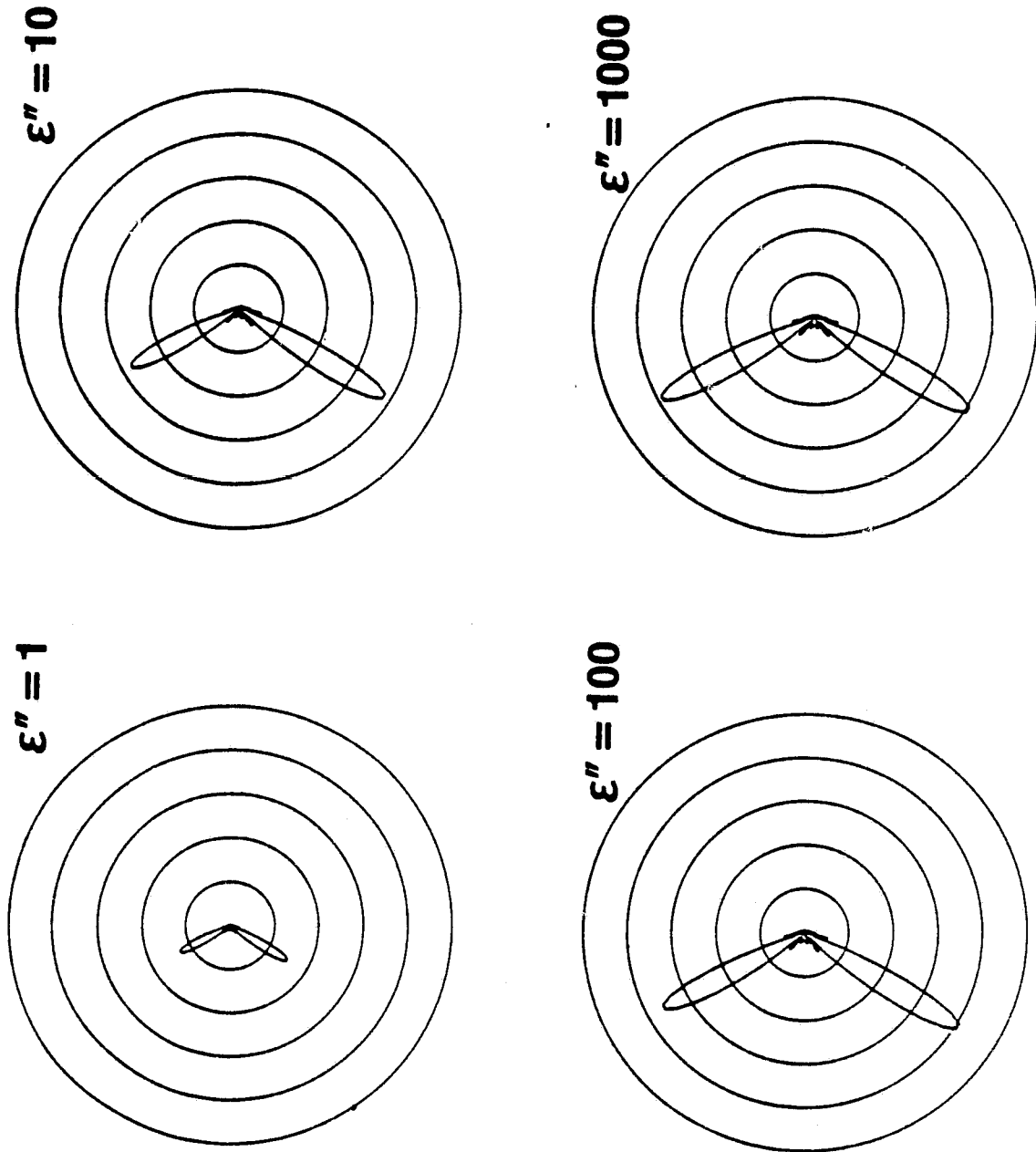
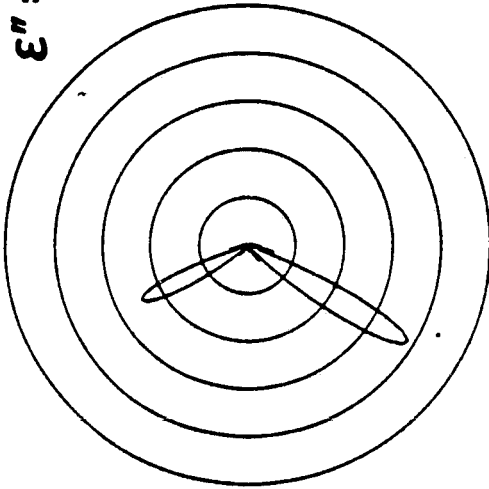
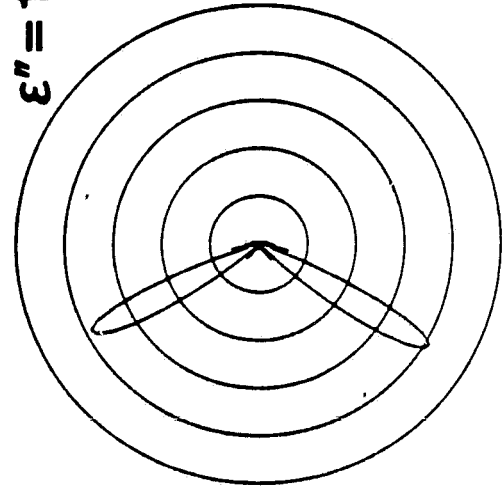


Figure 14. Magnitude of the scattering amplitude,  $f_{hh}$ , in the plane of incidence for purely lossy dielectric:  $\tilde{\epsilon}_f = j\epsilon''$ .

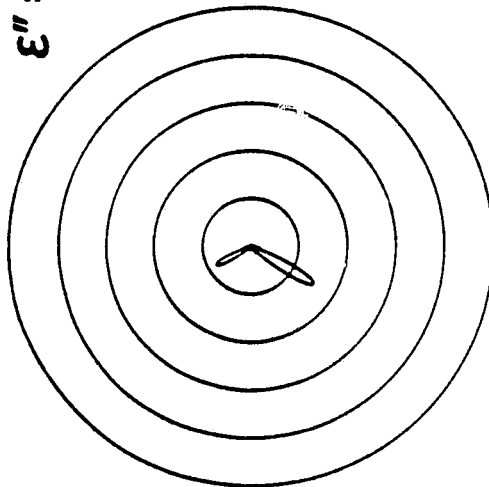
$\epsilon'' = 10$



$\epsilon'' = 1000$



$\epsilon'' = 1$



$\epsilon'' = 100$

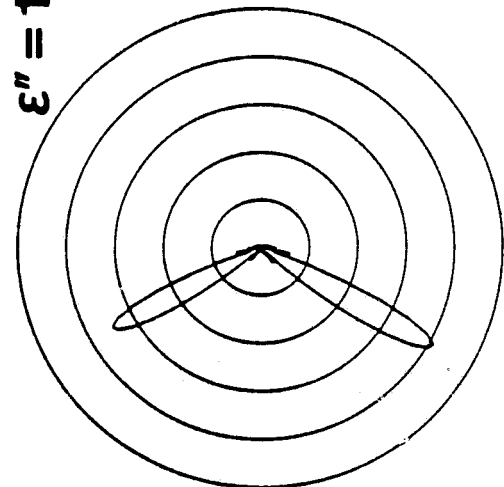


Figure 15. Magnitude of the scattering amplitude,  $f_w$ , in the plane of incidence for purely lossy dielectric:  $\hat{\epsilon}_T = j\epsilon''$ .

ORIGINAL PAGE IS  
OF POOR QUALITY.

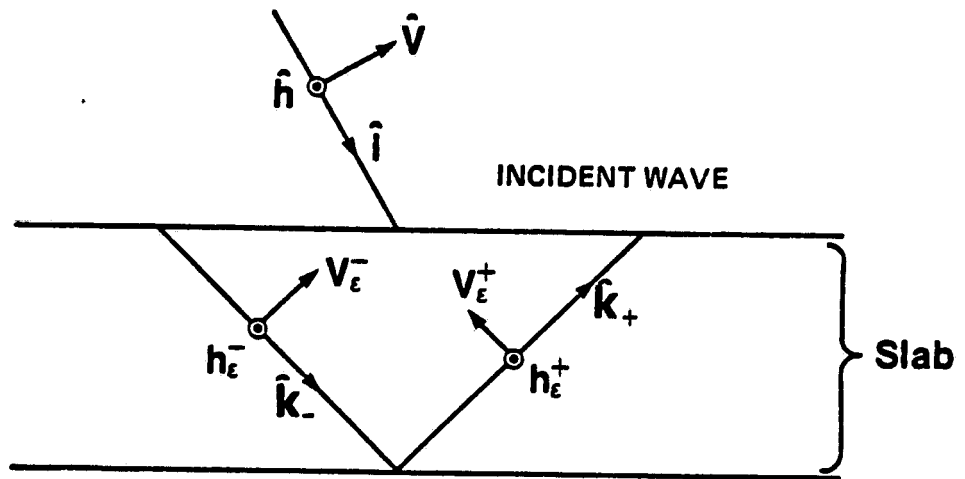


Figure 16. Polarization and propagation vectors inside the slab.